

michigan state university Libraries

3 1293 00558 4879

LIBRARY Michigan State University

This is to certify that the

thesis entitled

Electron Emission and Single Crystal

X-Ray Diffraction Studies

of Alkalides and Electrides

presented by

Rui He Huang

has been accepted towards fulfillment of the requirements for

Ph.D. degree in Chemistry

Major professor

Date \_\_\_\_\_12/11/87

MSU is an Affirmative Action/Equal Opportunity Institution

**O**-7639



RETURNING MATERIALS:
Place in book drop to remove this checkout from your record. FINES will be charged if book is returned after the date stamped below.

# ELECTRON EMISSION AND SINGLE CRYSTAL X-RAY DIFFRACTION STUDIES OF ALKALIDES AND ELECTRIDES

By

Rui He Huang

A DISSERTATION

Submitted to

Michigan State University

in partial fulfillment of the requirements

for the degree of

DOCTOR OF PHILOSOPHY

Department of Chemistry

#### **ABSTRACT**

## ELECTRON EMMISION AND SINGLE CRYSTAL X-RAY DIFFRACTION STUDIES OF ALKALIDES AND ELECTRIDES

By

#### Rui He Huang

The crystal structures of an electride, K+(C222).e-, and five alkalides,  $Cs^+(18C6)_2.Cs^-$ ,  $Cs^+(C222).Cs^-$ ,  $Rb^{+}(C222).Rb^{-}$ ,  $K^{+}(C222).Na^{-}$  and  $Cs^{+}(15C5)_{2}.K^{-}$ , were determined. The structure of K+(C222).e provides evidence of electron pairing, consistent with other properties of this electride. The long (in Cs + (18C6) 2.Cs - ) and short (in Cs + (C222).Cs -) uniform chain packing of ceside anions in both cesides explains the presence of a Cs solid state NMR peak in Cs<sup>+</sup>(18C6)<sub>2</sub>.Cs<sup>-</sup> and its absence in Cs<sup>+</sup>(C222).Cs<sup>-</sup>. A dimer-type species,  $Rb_2^{2-}$ , was found for the first time in Rb+(C222).Rb-. The minimum and the effective radii obtained from these structures are: 2.55 and 2.73 Å for Na, 2.80 and 3.15 A for K, 3.0 and 3.2 A for Rb and 3.1 and 3.5 A for Cs .

Photoemission studies of alkalides and electrides were made by quantum yield spectra. The photoemission peaks for the alkali metal anions are: 300 and 330 nm for Na<sup>-</sup>, 370 nm for K<sup>-</sup> and 380 nm for Rb<sup>-</sup>. Quantum yields are strongly temperature dependent. Trace amount of Na contamination from Pyrex glassware has a great effect on the photoemission quantum yield spectra of electrides and alkalides other than sodides.

Thermionic emission was observed from crystals and films of alkalides and electrides at temperatures as low as -60 °C. The temperature dependence of emission currents follows the Richardson-Dushman equation and the Richardson plots of the thermionic emission from crystals or films yield work functions of only a few tenths of an eV.

## TO MY PARENTY

#### ACKNOWLEDGEMENT

I wish to express my sincere appreciation to Dr. James L. Dye for his guidance and support through the whole course of my research project.

I would like to thank all the members of Dr. Dye's group with whom I have worked, in particular Steve Dawes, Margie Faber, Mary Tinkham, Odette Fussa, Ahmed Ellaboudy, Zheng Li, Francoise Tientega, Mark Kuchenmeister, Joe Skowyra, Lauren Hill, Jineun Kim, Judy Eglin and Kevin Moeggenborg for their cooperation, suggestions and discussions. The warm atmosphere in the group has made my research much more enjoyable.

My special acknowledgement goes to Dr. Don Ward, who has played a major role in the single crystal structure determination, Deak Watters, who has constructed the vacuum chamber for photoemission, and Martin Rabb, who designed and constructed the electronic system for the photoemission study.

I would like to thank the glassblowers Scott Bancroft,
Manfred Langer and Keki Mistry for their excellent service
and the instrument makers Russ Geyer and Dick Menke for

their help in my research work. I want to thank Shin-Chu Hsu and Dean Peterson for their help in microwave measurements.

I would also like to thank my parents for their encouragement and assistance, without which my study in U.S. would be impossible, and my wife Xiao Zhen Li for her support and understanding.

I am grateful for financial support from the Chemistry Department, Michigan State University, the National Science Foundation (grant DMR 84-14154 and grant DMR 84-03494) and the Monsanto research fellowship.

## TABLE OF CONTENTS

		Page
LIST OF	TABLES	
LIST OF	FIGURES	
CHAPTER	ONE: INTRODUCTION	1
CHAPTER	TWO: CRYSTAL STRUCTURE DETERMINATION	5
	1. Experimental	5
	2. Crystal structure of K <sup>+</sup> (C222).e <sup>-</sup>	8
	3. Crystal structure of Cs <sup>+</sup> (18C6) <sub>2</sub> .Cs <sup>-</sup>	
	and Cs <sup>+</sup> (C222).Cs <sup>-</sup>	21
	4. Crystal structure of Rb <sup>+</sup> (C222).Rb <sup>-</sup>	30
	5. Crystal structure of K <sup>+</sup> (C222).Na <sup>-</sup>	34
	6. Crystal structure of Cs <sup>+</sup> (15C5) <sub>2</sub> .K <sup>-</sup>	40
CHAPTER	THREE: PHOTOEMISSION OF ALKALIDES AND ELECTRIDES	44
	3.1 Background	44
	3.2 Experimental	54 .
	3.2.1 Experimental system	54
	A. Photoemission chamber	54
	B. Optical system	56
	C. Vacuum system	56
	D. Solvent system	56

E. Electronic system	•	•	•	•	•	56
3.2.2 Experimental procedure	•	•	•	•	•	56
A. Film making	•	•	•	•	•	56
B. Quantum yield measuremen	t	•			•	57
C. EDC measurement	•	•	•	•	•	58
3.3 Results and discussion		•	•			58
CHAPTER FOUR: THERMIONIC EMISSION FROM ALK	ΔT.	מד	ES			
AND ELECTRIDES						69
CHAPTER FIVE: SUMMARY AND CONCLUSIONS	•	•	•	•	•	78
APPENDICES						
APPENDIX 1: CRYSTAL STRUCTURE DATA OF K <sup>+</sup> (C2 Cs <sup>+</sup> (18C6) <sub>2</sub> .Cs <sup>-</sup> , Cs <sup>+</sup> (C222).Cs <sup>-</sup> ,	22	).	e <sup>-</sup>			
Rb <sup>+</sup> (C222).Rb <sup>-</sup> ,K <sup>+</sup> (C222).Na <sup>-</sup>						
and Cs <sup>+</sup> (15C5) <sub>2</sub> .K <sup>-</sup>						80
			•	•	•	
APPENDIX 2: EXPLANATION OF THE ENTRIES IN T TABLES OF CRYSTAL DATA			•		•	102
TICH OF DEFENDENCES						104

## LIST OF TABLES

TABLE		PAGE
2-1	Recrystallization Parameters	. 7
2-2	Microwave Absorption Measurement	. 11
2-3	Crystal Data of K <sup>+</sup> (C222).e <sup>-</sup>	. 13
2-4	Crystal Data of Cs <sup>+</sup> (18C6) <sub>2</sub> .Cs <sup>-</sup>	. 24
2-5	Crystal Data of Cs <sup>+</sup> (C222).Cs <sup>-</sup>	. 26
2-6	Crystal Data of Rb (C222).Rb	. 31
2-7	Crystal Data of K+(C222).Na	. 38
2-8	Crystal Data of Cs <sup>+</sup> (15C5) <sub>2</sub> .K <sup>-</sup>	41
A-1	Table of Positional Parameters and Their	
	Estimated Standard Deviations for Potassium	
	Cryptand [2.2.2] Electride	. 81
A-2	Table of Bond Distances (in Angstroms) for	
	Potassium Cryptand [2.2.2] Electride	. 83
B-1	Table of Positional Parameters and Their	
	Estimated Standard Deviations for Cesium	
	(18-Crown-6) <sub>2</sub> Ceside	86
B-2	Table of Bond Distances (in Angstroms) for	
	Cesium (18-Crown-6) Ceside	. 87

C-1	Table of Positional parameters and their
	Estimated Standard Deviations for Cesium
	Cryptand [2.2.2] Ceside 90
C-2	Table of Bond Distances (in Angstroms) for
	Cesium Cryptand [2.2.2] Ceside 91
D-1	Table of Positional Parameters and Their
	Estimated Standard Deviations for Rubidium
	Cryptand [2.2.2] Rubidide
D-2	Table of Bond Distances (in Angstroms) for
	Rubidium Cryptand [2.2.2] Rubidide 94
E-1	Table of Positional Parameters and Their
	Estimated Standard Deviations for
	K <sup>+</sup> (Cryptand[2.2.2]).Na <sup>-</sup>
E-2	Table of Bond Distances (in Angstroms) for
	K <sup>+</sup> (Cryptand[2.2.2]).Na <sup>-</sup>
F-1	Table of Positional Parameters and Their
	Estimated Standard Deviations for Cesium
	(15-Crown-5) <sub>2</sub> Potasside
F-2	Table of Bond Distances (in Angstroms) for
	Casium (15-Crown-5) Potassida 100

### LIST OF FIGURES

FIGURE		PAGE
2-1	Molar electronic susceptibility of	
	K(C222).e . Obtained from the overall	
	susceptibility by subtracting the	
	susceptibility of the decomposed sample	
	and the low temperature Curie-law	
	paramagnetism. Symbols are as follows:	
	x from reference [15]. o from this work	. 9
2-2.	Complexed cation hexagonal packing	
	patterns on an $\underline{a}-\underline{b}$ plane in $K^+(C222).e^-$	
	obtained by the Evans and Sutherland PS-300	
	display system	15
2-3.	Cross section of the $\underline{A}-\underline{A}$ plane in Figure	
	2-2 showing the channels along the $\underline{z}$ - and	
	$\underline{x}$ -axis in $K^+$ (C222).e <sup>-</sup> . The channels along	
	the $\underline{x}$ -axis appear rather small in this view.	17
2-4.	A cross section of the $\underline{B}-\underline{B}$ plane in	
	Figure 2-2 showing the channels along the	
	$\underline{z}$ - and $\underline{x}$ -axis. The intersection is	
	clearly shown and the channels along the	

	$\underline{x}$ -axis are large in this view. The alternate	
	$\underline{x}$ -channels appear closed in this view but	
	would appear open if the view displaced by	
	about 3 Å along the y-axis	. 8
2-5.	Cross sections of an intersection of	
	channels in K <sup>+</sup> (C222).e <sup>-</sup> . These cross	
	sections are perpendicular to the "long	
	axis" of the intersection	. 9
2-6.	Cross sections of an intersection of	
	channels in K <sup>+</sup> (C222).e <sup>-</sup> . These cross	
	sections are parallel to the "long axis"	
	of the intersection and perpendicular to	
	the <u>x</u> - <u>z</u> plane	!C
2-7.	Cross section of the narrowest section of	
	a channel along the $\underline{x}$ -axis connecting two	
	intersections in K <sup>+</sup> (C222).e <sup>-</sup> 2	2
2-8.	A thin section on the $\underline{b}-\underline{c}$ plane of the	
	Cs(18C6) <sub>2</sub> .Cs structure showing the ionic	
	chain packing	9
2-9.	A thin section on the $\underline{b}-\underline{c}$ plane of the	
	Cs <sup>+</sup> (C222).Cs <sup>-</sup> structure showing the ionic	
	chain packing	9
2-10.	A thin section on the $\underline{b}-\underline{c}$ plane of the	
	Rb <sup>+</sup> (C222).Rb <sup>-</sup> structure showing the	
	formation of the dimer $Rb_2^{2-}$	5

2-11.	A thin section of the structure of	
	Rb <sup>+</sup> (C222).Rb <sup>-</sup> in the a-b plane showing	
	the hexagonal-type packing patterns	
	similar to those in $K^+(C222).e^-$	36
3-1.	Photoexcitation of electrons from a solid	
	by photons of energy $\hbar\omega$ . $\phi$ is the	
	workfunction, $E_{vac}$ is the energy of the	
	vacuum level, E <sub>kin</sub> is the kinetic energy	
	of emitted electrons, $E_{\overline{F}}$ is the Fermi	
	energy	46
3-2.	Illustration of the fact that the density	
	of electronic states distribution of the	
	emitter, part (a), is reflected in the	
	photoemission spectral fine structure,	
	part (b). [ref.32]	46
3-3.	Energy dependence of the escape depth of	
	excited electrons showing the mean free	
	path as a function of kinetic energy.	
	[Ref.34]	49
3-4.	Quantum yield spectrum of a clean copper	
	surface. [Ref.42]	52
3-5.	Photoemission cell for studying the	
	photoemission of sodides. [Ref.10]	53
3-6.	Photoemission experimental system used	
	in this work	5/

3-7.	Quantum yield spectra of K <sup>+</sup> (15C5) <sub>2</sub> .K <sup>-</sup>	
	showing the effect of Na contamination.	
	Solid curve, synthesized in a Pyrex	
	cell. Dashed curve, synthesized in a	
	quartz cell	61
3-8.	Quantum yield spectrum of K <sup>+</sup> (15C5) <sub>2</sub> .K <sup>-</sup> at	
	-37 °C	62
3-9.	Quantum yield spectrum of Na <sup>+</sup> (C222).Na <sup>-</sup>	
	at -17°C	63
3-10.	Quantum yield spectrum of Rb <sup>+</sup> (15C5) <sub>2</sub> .Rb <sup>-</sup>	
	at -40°C	64
3-11.	Quantum yield spectrum of $K^+(15C5)_2.e^-$ at	
	-32°C	66
3-12.	Temperature dependence of quantum yield	
	of K <sup>+</sup> (15C5) <sub>2</sub> .K <sup>-</sup>	67
4-1.	Thermionic emission current signal during	
	film making of $K^+(15C5)_2.K^-$ . MeNH <sub>2</sub> was used	
	as solvent. The temperature was about -60°C.	71
4-2.	Saturation curve of the thermionic emission	
	current for a film of Rb <sup>+</sup> (15C5) <sub>2</sub> .Rb <sup>-</sup>	
	at -30°C	73
4-3.	Richardson plot of the thermionic emission	
	of K <sup>+</sup> (15C5)e <sup>-</sup> from film (a) and	

	crystals (b)	75
4-4.	Diagram showing the electron distribution	
	in the Wigner-Seitz spheres and the	
	effects of electron spill-out and smooth-	
	out near a surface. [Ref.31]	76
A-1	Drawing of single molecule of	
	K <sup>+</sup> (C222).e <sup>-</sup>	85
A-2	Stereoview of the unit cell of	
	K <sup>+</sup> (C222).e <sup>-</sup>	85
B-1	Drawing of single molecule of	
	Cs <sup>+</sup> (18C6) <sub>2</sub> .Cs <sup>-</sup>	89
B-2	Stereoview of the unit cell of	
	Cs <sup>+</sup> (18C6) <sub>2</sub> .Cs <sup>-</sup>	89
C-1	Drawing of single molecule of	
	Cs <sup>+</sup> (C222).Cs <sup>-</sup>	92
C-2	Stereoview of the unit cell of	
	Cs <sup>+</sup> (C222).Cs <sup>-</sup>	92
_	Drawing of single molecule of	
	Rb <sup>+</sup> (C222).Rb <sup>-</sup>	95
D-2	Stereoview of the unit cell of	
	Rb <sup>+</sup> (C222).Rb <sup>-</sup>	
<b>7</b> 4		95
E-1	Drawing of single molecule of	
	K <sup>+</sup> (C222).Na <sup>-</sup>	98
E-2	Stereoview of the unit cell of	

	K <sup>+</sup> (C222).Na <sup>-</sup> 9
F-1	Drawing of single molecule of
	Cs <sup>+</sup> (15C5) <sub>2</sub> .K <sup>-</sup>
F-2	Stereoview of the unit cell of
	Cs <sup>+</sup> (15C5) <sub>2</sub> .K <sup>-</sup>

#### CHAPTER 1

#### INTRODUCTION

Alkalides and electrides are two new classes of compounds discovered and studied in Dr. Dye's laboratory at Michigan State University during the last decade [1-4]. Twenty five alkalides and five electrides have been synthesized and characterized to date [5]. These unique ionic compounds consist of alkali metal cations shielded by large cyclic or bicyclic polyether or polyamine ligands and either large alkali metal anions, in which electrons are in filled S<sup>2</sup> orbitals, or electrons trapped at anionic sites. Because of the weak electron binding, it is not surprising that these crystalline compounds have some unusual chemical and physical properties.

Much work has been focussed on studies of these compounds by optical spectra, chemical analysis, NMR, EPR, magnetic susceptibility, DC conductivity and other techniques [3]. However, the research in two key fields, crystal structure and band structure, had been hindered by the difficulty of handling these compounds. The first alkalide, Na<sup>+</sup>(C222).Na<sup>-</sup> (C222=cryptand [222]), was synthesized and characterized

in 1974 [1] and the crystal structure was determined soon after the synthesis [2]. Since then many new alkalides and electrides have been discovered [3,5]. However, over a ten year period, many attempts to determine the crystal structures of other alkalides and of electrides failed because of the high reactivity of these compounds with air and/or moisture and the tendency towards irreversible decomposition at temperatures above about -40 °C. Meanwhile, an EXAFS study of alkalides and electrides that contained rubidium was carried out to obtain some structural information [8,27]. However, only qualitative information about the structures could be obtained from the EXAFS experiments. In 1985, a new technique for growing and handling suitable single crystals was established in our laboratory by S. Dawes and O. Fussa, following the suggestions of Professors H. Hope and D. Powers of the University of California at Davis [6,7,8]. Since then, more than 10 crystal structures of alkalides and electrides have been determined, and this achievement has greatly advanced our understanding of the properties of these novel compounds [11,12,13]. In the present work, the crystal structures of one electride and five alkalides were determined and are reported.

Despite the difficulty of handling these compounds, studies in our laboratory prior to the present work had given us some information about the electronic band

structures of alkalides and electrides. This information can be summarized as follows:

- 1. The optical spectra of thin films of alkalides and electrides showed optical absorption peaks for Na, K, Rb and Cs at about 650, 800, 860 and 950 nm respectively [3,4,5]. These optical bands may represent the transitions from the S<sup>2</sup> ground states to the S<sup>1</sup>P<sup>1</sup> excited states of the anions. For a localized electride, such as Cs (18C6)<sub>2</sub>.e (18C6=18crown6), a peak appeared at about 1.6 micrometers [14]. Some electrides, such as K (C222).e and Li (C211).e, showed plasma-type spectra indicating different types of electron trapping [15,16]. Little was known about the band structures of electrides.
- 2. Powder DC conductivity measurements showed that most of the alkalides and electrides behave as semiconductors with band gaps ranging from 2.5 eV to a few tenths of an eV [3,4]. Since most of the alkalides contain some trapped electrons, which are believed to lie closer to the conduction band than do the alkali anions, the conductivities are dominated by the electride impurities and the apparent band gaps are about 0.5 to 1.0 eV. Na<sup>+</sup>(C222).Na<sup>-</sup> is an exception. It can crystallize in rather pure form with very low concentration of trapped (or defect) electrons. Recent measurements of powder and single crystal

DC conductivity of  $Na^+(C222).Na^-$  showed that the band gap in this compound is  $2.4 \pm 0.2$  eV [9].

3. Preliminary studies of photoemission of sodides showed that sodide films had two major quantum yield peaks at 650 and 370 nm. They were assigned to the photoemissions from trapped electrons and the sodide ion, Na, respectively [10]. The quantum yield was a strongly temperature-dependent function and the mechanism was unknown.

Photoemission is known as the most powerful tool for studying band structure in solids. A part of the present work was to continue the work on photoemission of alkalides and electrides.

#### CHAPTER 2

#### CRYSTAL STRUCTURE DETERMINATION

Single crystal X-ray diffraction is one of the most powerful methods for understanding the properties of alkalides and electrides. Crystal structure determinations enable us to understand, and sometimes to predict, the electronic, magnetic, optical and other properties of these compounds. Sometimes it is the best way to determine the chemical stoichiometry. For example, it was thought that there was only an electride Cs<sup>+</sup>(C222).e<sup>-</sup> in the Cs-C222 system because no Cs<sup>-</sup> NMR signal has been found in the system [14]. But the x-ray diffraction experiment in this work showed that there was a ceside, Cs<sup>+</sup>(C222).Cs<sup>-</sup>.

### 1.Experimental.

Although there are many ways of growing single crystals, all single crystals used in this work were grown by the temperature scanning technique. Polycrystalline samples used

for crystal growing were synthesized by the methods mentioned elsewhere [3,5]. A two-chamber apparatus for recrystallization was used. After the polycrystalline sample had been loaded into the apparatus at low temperature under a nitrogen atmosphere, the apparatus was pumped on a vacuum line, while been kept cold in a Dry-Ice bath, and dimethyl ether (DME) was introduced to dissolve the crystals. Then a co-solvent (trimethyl amine (TMA) or diethyl ether (DEE)) was distilled into the apparatus to form a mixed solvent solution in order to reduce the solubility. A saturated solution with some seed crystals was made by distilling out some of the solvent at the temperature at which crystal growing was to start. Then the apparatus was transferred to a thermal bath through which cold alcohol was circulated by a programmable NESLAB LT-9 bath. The cooling rate could be varied from 2 degrees/hour to .25 degrees/hour. After the temperature had been scanned according to the program and reached the lowest value, the mother liquor was poured into the other side and all of the solvents were distilled out, and the dry crystals were kept at dry-ice temperature until used. Usually 3 sets of samples were made simultaneously with the hope that one set would yield some good single crystals.

The recrystallization conditions are summarized in Table 2-1.

TABLE 2-1. RECRYSTALLIZATION CONDITIONS

Compound	Solvent	Temperature	Scan Time	Procedure
	System	Scan Range	(hours)	
Cs <sup>+</sup> (18C6) <sub>2</sub> .Cs <sup>-</sup>	DME/TMA	-4256 °C	10	down-up-
_				down
Cs <sup>+</sup> (C222).Cs <sup>-</sup>	DME/TMA	-4263 °C	10	down-up-
				down
Cs <sup>+</sup> (15C5) <sub>2</sub> .K <sup>-</sup>	DME/TMA	-3567 °C	50	down
Rb <sup>+</sup> (C222).Rb <sup>-</sup>	DME/DEE	-4267 °C	50	down
K <sup>+</sup> (C222).Na <sup>-</sup>	DME/TMA	-3967 °C	50	down
+				
K <sup>+</sup> (C222).e <sup>-</sup>	DME/DEE	-5067 °C	50	down

The techniques for examining and mounting single crystals have been described in detail by S. Dawes [7] and O. Fussa [8].

A Nicolet P3F diffractometer with an LT-1 low temperature device was used for data collection. The temperature of the crystals could be varied between -60 and -80°C.

The detailed crystal structure data ( single molecule diagram, packing diagram, positional and thermal parameters, bond distances, etc. ) of each structure can be found in the Appendices. Complete crystal data for each structure are published in the separate papers [26].

## 2. Crystal structure of K<sup>+</sup>(C222).e<sup>-</sup>.

It was of great interest to determine the crystal structure of  $K^+(C222).e^-$  because evidence showed that it might be a delocalized electride or a spin-paired electride. The optical absorption spectrum of thin films of the compound showed a plasma-type spectrum similar to that in alkali metal-ammonia solutions and the magnetic susceptibility data showed that it had a weak paramagnetic Curie tail at low temperature ( < 5 K) corresponding to less than 1% free electrons and then the susceptibility increased slowly with temperature up to 200 K [5,12,15]. Figure 2-1 shows the molar electronic susceptibility of  $K^+(C222).e^-$  obtained by M. Faber [15] and in this work. Although the paramagnetic Curie tails in the two runs are

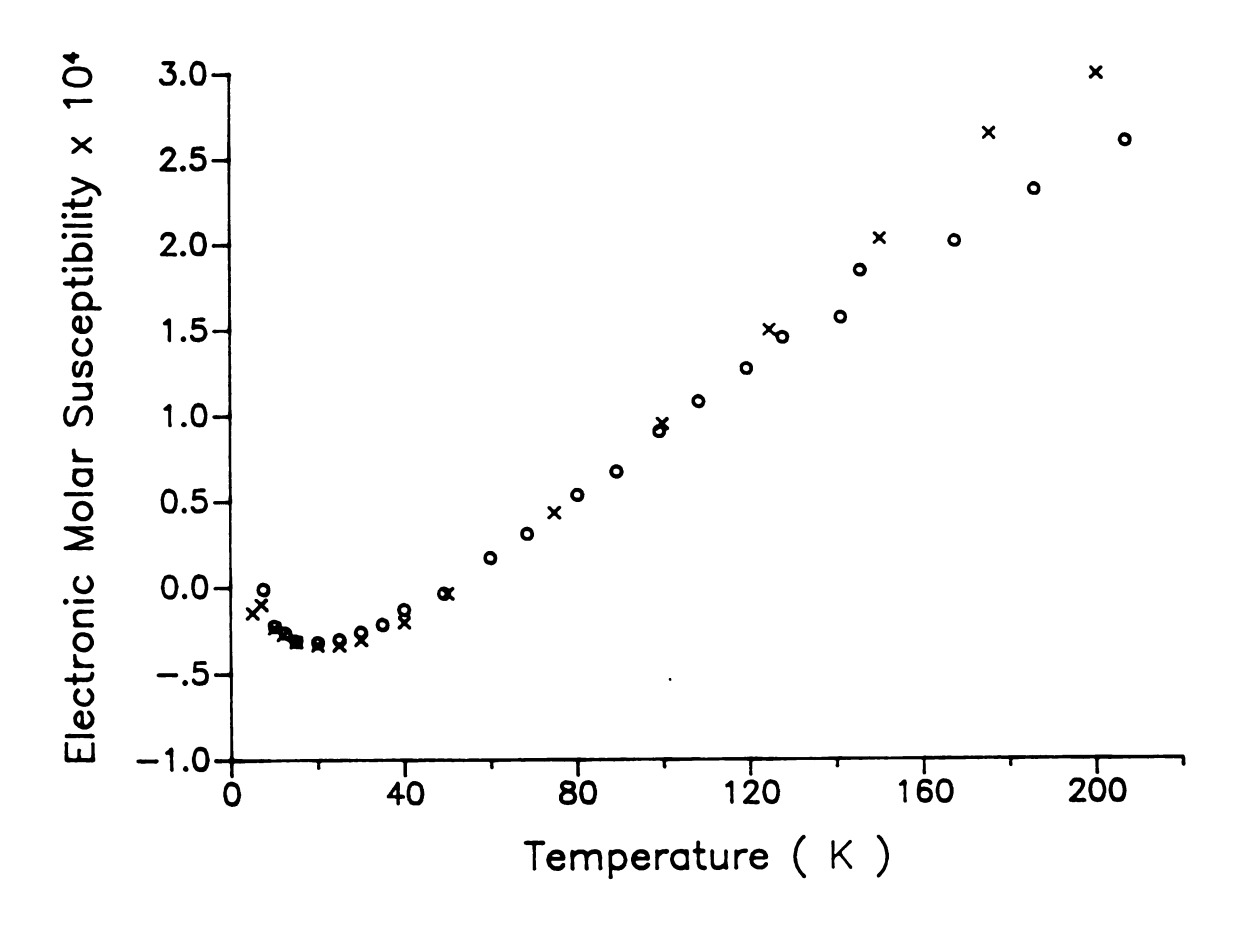


Figure 2-1. Molar electronic susceptibility of K(C222).e. Obtained from the overall susceptibility by subtracting the susceptibility of the decomposed sample and the low temperature Curie-law paramagnetism. Symbols are as follows: x from reference [15]. o from this work.

rather different ( 1% and .5% unpaired spins ), the molar electronic susceptibilities in both measurements are remarkably close after the susceptibility of the decomposed sample ( diamagnetic contribution ) and the Curie paramagnetism were subtracted from the total susceptibility. The microwave conductivity measurement showed that this compound had a microwave conductivity similar to a powdered metal Zn ( Table 2-2 ). Powder D.C. conductivity measurement of this electride have been unsuccessful for years. However, some successful experiments have been recently carried out which show that the electride K+(C222).e behaves as a semiconductor with a positive temperature coefficient of conductivity [12]. However, the activation energy is less than one tenth of an eV. All of these properties are so different from that of the electride Cs + (18C6)2.e whose structure has been previously determined [6] that one should expect the electron trapping sites in these two electrides to be very different. The electride K+(C222).e behaves as an electride with electron pairs trapped in very shallow sites.

The parameters of recrystallization are shown in Table 2-1. Because of its tendency towards decomposition at rather low temperature ( $-40\,^{\circ}\text{C}$ ), recrystallization had to be done at temperatures lower than  $-50\,^{\circ}\text{C}$ . The single crystals were black in color and flat with the dimensions of a few mm in two directions (the <u>a</u> and <u>c</u> axes). The crystal data are

Table 2-2. Microwave Absorption Measurements

Microwave Frequency : X-band, 9.0 GHz

Temperature : -85 °C

Tubing : 3mm OD quartz

Sample	Transmission Signal
	(arbitrary scale, mV on detector)

Empty tube	80
Cu (powder)	3.5
Zn (powder)	7
Na + (C222). Na -	78
Cs <sup>+</sup> (18C6) <sub>2</sub> .e <sup>-</sup>	78
K <sup>+</sup> (15C5) <sub>2</sub> .e <sup>-</sup>	74
Rb <sup>+</sup> (C222).e <sup>-</sup>	42
K <sup>+</sup> (C222).e <sup>-</sup>	10

summarized in Table 2-3. The structure confirmed that the electride consists of complexed cations and "empty" spaces containing only noise level electron density. The structure of the cryptated cation K<sup>+</sup>(C222), which has K<sup>+</sup>-O distances ranging from 2.795 to 2.858  ${\rm \AA}$  and  ${\rm K}^+$ -N distances of 2.958 and 2.981 Å, is similar to that in the salt  $K^+(C222).I^-$ [23]. In order to study the correlation of the electride structure with its properties we need to investigate the shape and the distribution of the "empty" spaces where the trapped electrons probably "reside". This was done by using an Evans and Sutherland PS-300 display system in which the a-axis of the crystal is taken to be the x-axis of the display in a right-handed x-y-z orthogonal system, and the <u>b</u>-axis of the crystal is located in the x-y plane. Therefore, the b-axis of a monoclinic crystal is taken as the y-axis. The van der Waal's surfaces of atoms and ions are used to display the packing, and channels in structures are bounded by the van der Waal's surfaces of the complexed cations and anions. Roughly speaking, the "empty" spaces form a two-dimensional network of channels along the z and  $\mathbf{x}$  axes in this electride. There are no continuous channels along the y-axis.

On the  $\underline{x}-\underline{y}$  plane the cryptated cations form hexagonal patterns with the cryptands interlocking into each other to form very efficient packing ( Figure 2-2 ). The vertical displacement of alternate cations of a hexagonal-type ring

Table 2-3. Crystal Data of K<sup>+</sup>(C222).e<sup>-\*\*</sup>

Crystal dimensions : 0.2 x 0.6 x 0.8 mm

Temperature : 202 K

Space group : monoclinic, C2/c

Cell paramaters : a=12.129(8), b=20.692(13),

c=21.519(16) Å, beta=95.23(6)°,

V=5378(6) Å<sup>3</sup>, Z=8

Peak width at

half-height : 0.30 degree

Scan type : theta - 2theta

Scan rate : 4 degrees/min. (in 2theta)

Maximum 2 theta : 45 degrees

No. of refl.measured: 6692

No. of unique refl. : 6394

No. of refl. used

in refinement :  $3614 \text{ with } \text{Fo}^2 > 3.0 \text{ sigma}(\text{Fo}^2)$ 

Corrections : Lorentz-polarization

Linear decay

(1.001 to 1.061 on I)

Reflection averaging (R<sub>int</sub>=1.7%)

Empirical absorption (0.92 to 1.00 on I)

Solution : Direct methods

## Table 2-3. (cont'd)

Hydrogen atoms : Located and refined isotropically

R : 0.041

R<sub>w</sub> : 0.040

High peak in final

diff. map : 0.10 (1)  $e/Å^3$ 

Low peak in final

diff. map :  $-0.11(1) e/Å^3$ 

Esd of obs. of

unit weight : 0.96

Convergence,

largest shift : 0.03 sigma

\*\* For the explanation of the entries in the table, see Appendix 2.

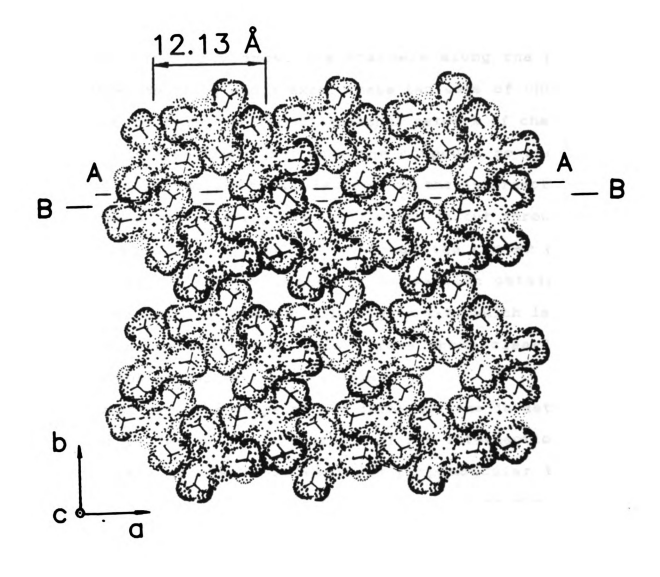


Figure 2-2. Complexed cation hexagonal packing patterns on an  $\underline{a}-\underline{b}$  plane in  $K^+(C222).e^-$  obtained by the Evans and Sutherland PS-300 display system.

is 1.7 Å (along the z-axis). At the center of each hexagonal ring there is a hexagonal-type channel going along the z-axis with a diameter of about 4 Å.

The channels along the  $\underline{z}$ -axis zigzag towards the  $\underline{x}$  (mainly) and the  $\underline{y}$  axes. The channels along the  $\underline{x}$ -axis zigzag towards the  $\underline{y}$  and  $\underline{z}$  axes. These two sets of channels intersect to form the two-dimensional network of channels. It is the intersections that make the compound so special. Figure 2-3 shows the cross section of the intersection of the channels in the  $\underline{x}$ - $\underline{z}$  plane (101) which is cut through the plane  $\underline{A}$ - $\underline{A}$  on the Figure 2-2 (through the center of the channel). Figure 2-4 is another cross section obtained by cutting through the plane  $\underline{B}$ - $\underline{B}$  in Figure 2-2, which is about 1.5  $\underline{A}$  from the plane  $\underline{A}$ - $\underline{A}$ . This figure shows clearly the intersection of two sets of channels.

To investigate the shape of the intersections in detail we took two series of cross sections of one intersection. One set consists of the cross sections perpendicular to its "long axis" ( The "long axis" is perpendicular to the  $\underline{x}$ -axis and at an angle of 40 degrees with the  $\underline{x}$ -axis in the  $\underline{x}$ - $\underline{z}$  plane. )( Figure 2-5). Another set consists of the cross sections parallel to the "long axis" and perpendicular to the  $\underline{x}$ - $\underline{z}$  plane ( Figure 2-6 ). These figures show that each intersection has a dumbbell shape with a long dimension of about 12 Å and 6x4 Å cross sections at both ends and 4x4 Å cross sections at the middle. The 6x4x4 Å site at each end of the dumbbell cavity is surprisingly close in volume to

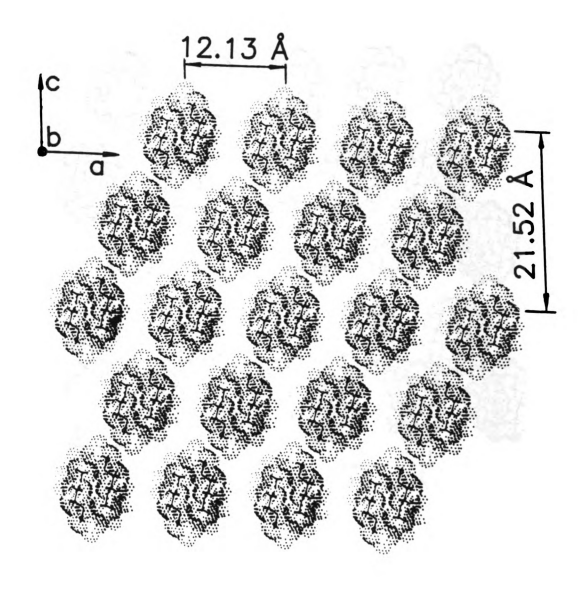


Figure 2-3. Cross section of the  $\underline{A}-\underline{A}$  plane in Figure 2-2 showing the channels along the  $\underline{z}$ - and  $\underline{x}$ -axis in  $K^+(C222).e^-$ . The channels along the  $\underline{x}$ -axis appear rather small in this view.

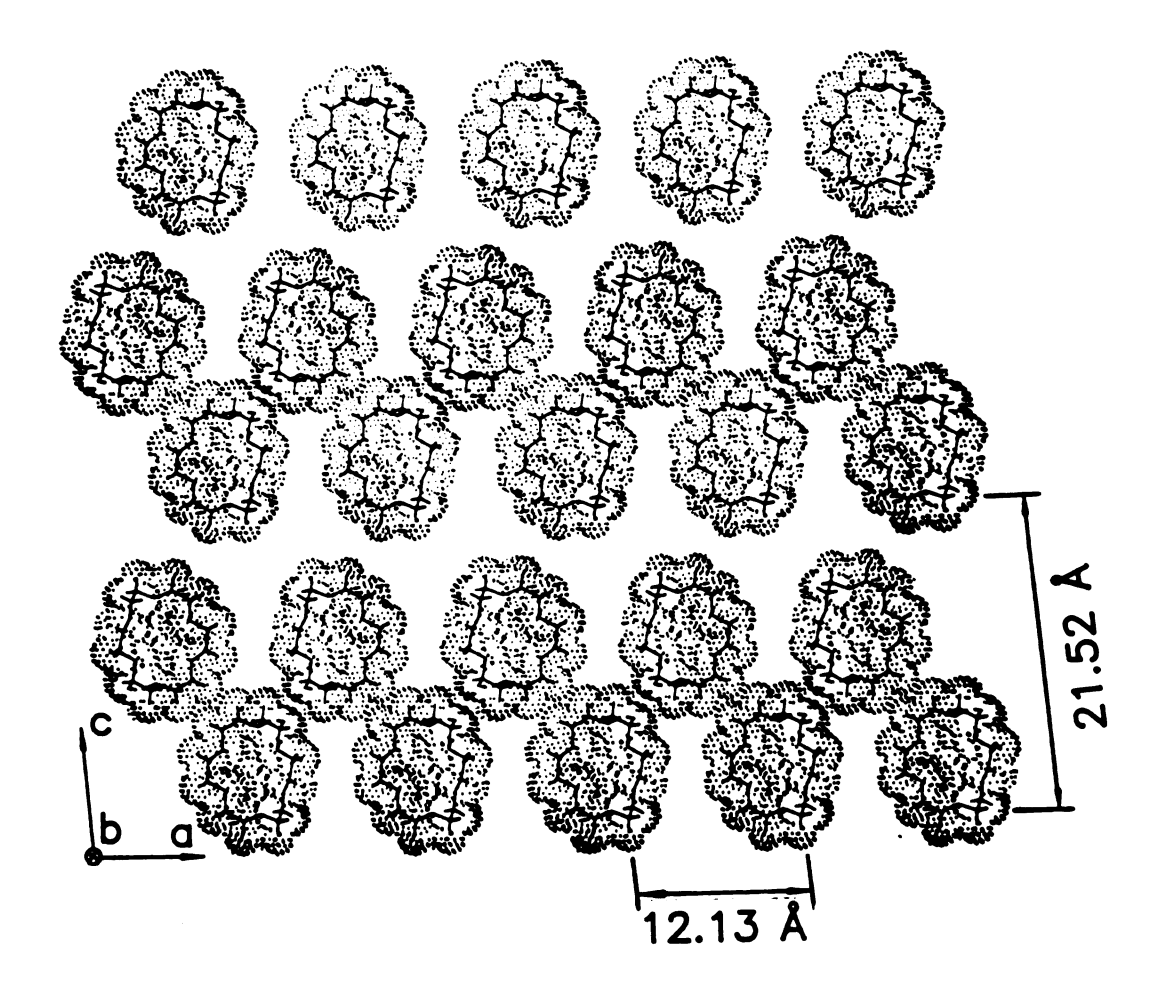


Figure 2-4. A cross section of the  $\underline{B}-\underline{B}$  plane in Figure 2-2 showing the channels along the  $\underline{z}-$  and  $\underline{x}-$ axis. The intersection is clearly shown and the channels along the  $\underline{x}-$ axis are large in this view. The alternate x-channels appear closed in this view but would appear open if the view displaced by about 3 Å along the y-axis.

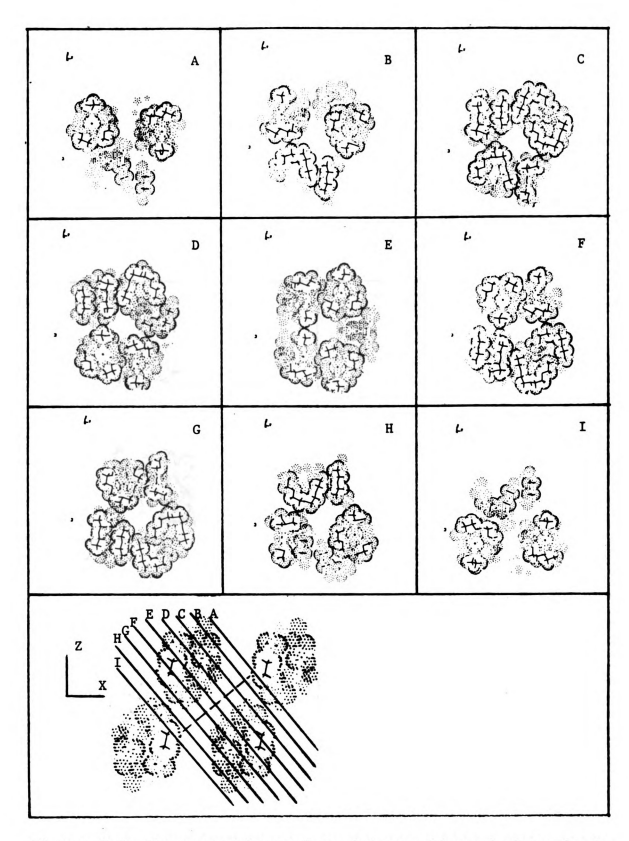


Figure 2-5. Cross sections of an intersection of channels in  $K^+(\text{C222}).e^-.$  These cross sections are perpendicular to the "long axis" of the intersection.

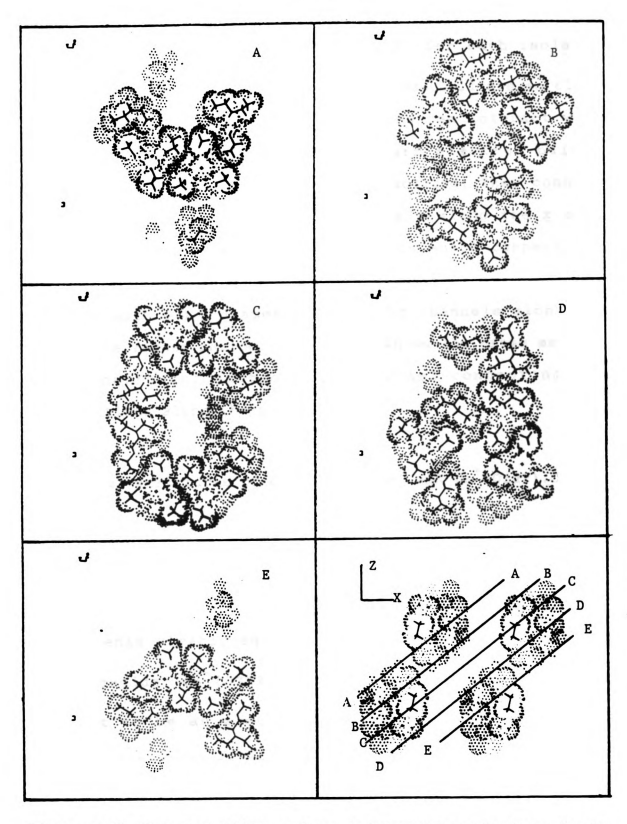


Figure 2-6. Cross sections of an intersection of channels in  $K^+(C222).e^-$ . These cross sections are parallel to the "long axis" of the intersection and perpendicular to the  $\underline{x-z}$  plane.

the trapping sites in  $Cs^+(18C6)_2.e^-$  [7] for each isolated trapped electron. The two sites in a dumbbell are so close to each other that the trapped electrons can interact with each other strongly enough to form electron pairs. Furthermore, these dumbbells are not isolated. They connect with each other through the channels along the  $\underline{z}$ -axis (mainly) and the  $\underline{x}$ -axis. The channels which connect the dumbbells along the  $\underline{z}$ -axis are rather uniform and hexagonal in shape with a 4 Å diameter. But, the channels along the  $\underline{x}$ -axis are rather narrow. Figure 2-7 shows the cross section at the narrowest section of a channel connecting two intersections along the  $\underline{x}$ -axis.

3. Crystal structures of Cs<sup>+</sup>(18C6)<sub>2</sub>.Cs<sup>-</sup> and Cs<sup>+</sup>(C222).Cs<sup>-</sup>.

Cs<sup>+</sup>(18C6)<sub>2</sub>.Cs<sup>-</sup> was the first ceside compound synthesized and characterized [17,18]. Optical and solid state NMR experiments clearly showed the existence of Cs<sup>-</sup>. But the second ceside, Cs<sup>+</sup>(C222).Cs<sup>-</sup>, was not identified and was thought to be an electride Cs<sup>+</sup>(C222).e<sup>-</sup> or mixture of electrides because no Cs<sup>-</sup> NMR signal was found in the Cs-C222 system [14]. Therefore it came as a surprise that the x-ray crystal structure data showed that the compound was a ceside Cs<sup>+</sup>(C222).Cs<sup>-</sup>.

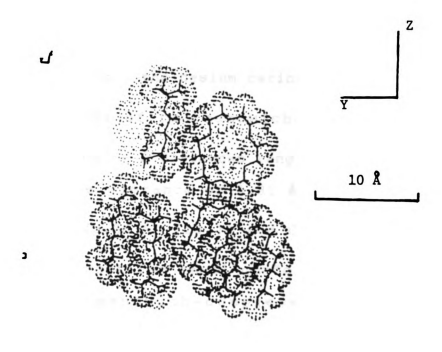


Figure 2-7. Cross section of the narrowest section of a channel along the  $\underline{x}$ -axis connecting two intersections in  $K^+(C222).e^-$ .

The recrystallization conditions for the preparation of these crystals are shown in Table 2-1.

Summaries of the crystal data are presented in Tables 2-4 and 2-5 for  $Cs^+(18C6)_2.Cs^-$  and  $Cs^+(C222).Cs^-$ , respectively.

In Cs<sup>+</sup>(18C6)<sub>2</sub>.Cs<sup>-</sup>, the cesium cation is coordinated to the 12 oxygen atoms of two sandwich-forming crown ether molecules with Cs + - O distances ranging from 3.113 to 3.516 A. The average distance of 3.31 A is close to those in  $Cs^{+}(18C6)_{2}.Na^{-}(3.36 \text{ Å})$  [19,7] and  $Cs^{+}(18C6)_{2}.e^{-}(3.35 \text{ Å})$ [6]. Thus , except for small conformational effects, the nature of the sandwich-complexed cesium cation is independent of the anion. The inclusive cesium cation in Cs<sup>+</sup>(C222).Cs<sup>-</sup> has six Cs<sup>+</sup>- O distances ranging from 2.89 to 2.99 Å, with two nitrogen atoms at 3.07 Å. Its structure is very similar to that in Cs<sup>+</sup>(C222).SCN<sup>-</sup>.H<sub>2</sub>O [20]. In both ceside structures , the cesium anions are in pockets lined with H atoms from the crown ethers or cryptands. The closest Cs<sup>-</sup>-H distances are 4.29 Å [Cs<sup>+</sup>(18C6)<sub>2</sub>.Cs<sup>-</sup>] and 4.37 Å [Cs<sup>+</sup>(C222).Cs<sup>-</sup>]. A hydrogen van der Waals radius of 1.2 Å yields a minimum radius of 3.1 Å. We expect Cs to be rather polarizable so that H atoms might penetrate somewhat into the outer electron density. The average distances of Cs to the 15 closest atoms ( all are H atoms ) are 4.66  $\hbox{\AA}$  Table 2-4. Crystal Data of Cs<sup>+</sup>(18C6)<sub>2</sub>.Cs<sup>-</sup>

Crystal dimensions :  $0.3 \times 0.4 \times 0.7 \text{ mm}$ 

Temperature : 204 K

Space group : orthorhombic, Pbca

Cell paramaters : a=16.212(8), b=16.374(6),

c=31.315(14) Å, V=8312(6) Å<sup>3</sup>, Z=8

Peak width at

half-height : 0.34 degree

Scan type : omega

Scan rate : 4 degrees/min (in omega)

Maximum 2 theta : 45 degrees

No. of refl.measured: 6585

No. of unique refl. : 5413

No. of refl. used

in refinement : 2221 with Fo<sup>2</sup> > 3.0 sigma(Fo<sup>2</sup>)

Corrections : Lorentz-polarization

Linear decay (1.022 to 1.146

on F)

Solution : Patterson method

Hydrogen atoms : ride on carbon atoms

## Table 2-4. (cont'd.)

R : 0.041

R<sub>W</sub> : 0.041

High peak in final

diff. map :  $0.48(7) e/\text{\AA}^3$ 

Low peak in final

**diff.** map :  $-0.37(7) \text{ e/Å}^3$ 

Esd of obs. of

unit weight : 1.27

Convergence,

largest shift : 0.08 sigma

Table 2-5. Crystal Data of Cs<sup>+</sup>(C222).Cs<sup>-</sup>

Crystal dimensions : 0.2 x 0.2 x 0.2 mm

: 206 K Temperature

Space group : monoclinic, P2,/n

Cell paramaters : a=13.371(2), b=11.252(2), c=21.529(3) Å, beta=94.80(1)°,

V=3227.7(9) Å<sup>3</sup>, Z=4

Peak width at

half-height : 0.27 degree

: Wyckoff w Scan type

8 degrees/min. (in omega) Scan rate

Maximum 2 theta : 45 degrees

No. of refl.measured: 4702

No. of unique refl. : 4211

No. of refl. used

in refinement :  $1418 \text{ with Fo}^2 > 2.0 \text{ sigma}(\text{Fo}^2)$ 

Lorentz-polarization Corrections

Linear decay (1.011 to 1.076

Reflection averaging

(R<sub>int</sub>=0.036)

: direct method Solution

### Table 2-5. (cont'd)

Hydrogen atoms : ride on carbon atoms

R : 0.071

R<sub>ut</sub> : 0.057

High peak in final

diff. map : 0.88(17) e/Å<sup>3</sup>

Low peak in final

diff. map :  $-0.93(17) e/Å^3$ 

Esd of obs. of

unit weight : 1.29

Convergence,

largest shift : 0.05 sigma

[Cs<sup>+</sup>(18C6)<sub>2</sub>.Cs<sup>-</sup>] and 4.70 Å [Cs<sup>+</sup>(C222).Cs<sup>-</sup>]. These yield an effective radius of 3.5 Å for Cs<sup>-</sup>, the biggest monatomic ion in nature!

The large size of Cs in both crystals makes the packing rather complicated. In Cs + (18C6) 2.Cs -, both the cations and the anions form zig-zag chains along the b-axis with uniform interionic distances of 8.78 Å and 8.86 Å respectively and each Cs is also 8.12 Å from another Cs in an adjacent chain. Figure 2-8 shows the ionic chain packing in Cs (18C6) 2.Cs. The "coordination shell" of each Cs is completed by seven complexed cations at distances of 8.09, 8.30, 8.31, 8.45, 9.28, 9.52 and 9.65 Å. In Cs<sup>+</sup>(C222).Cs<sup>-</sup>, the most striking feature of the ion-packing is the very short , uniform Cs -Cs distances of 6.38 Å in zig-zag chains parallel to the b-axis showing that the anions are in contact. This feature can be seen in Figure 2-9. The resulting distortion of the outer 6S wavefunction may broaden the Cs NMR signal beyond detection limits. This may be the reason for the absence of a Cs signal in the solid state NMR spectrum of the compound. In addition to the two adjacent anions in the chain, each Cs has nine neighboring cryptated Cs<sup>+</sup> ions at 7.13, 8.10, 8.60, 8.83, 8.89, 8.97,

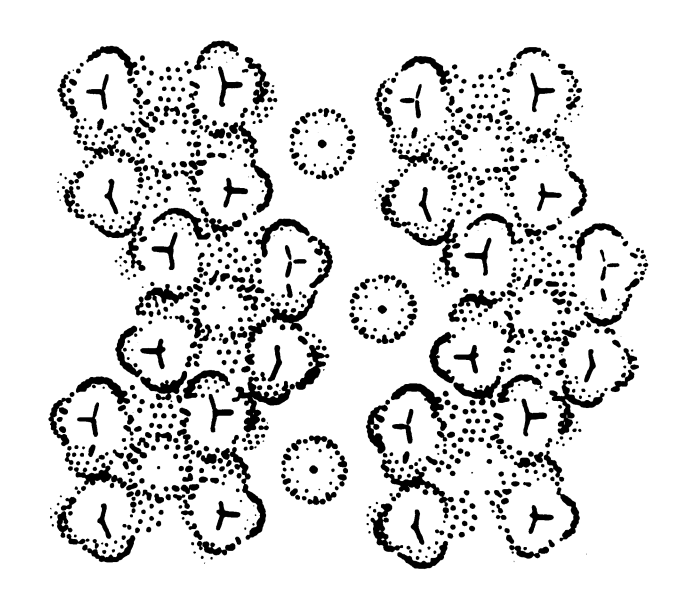


Figure 2-8. A thin section on the <u>b-c</u> plane of the  $Cs(18C6)_2.Cs^-$  structure showing the ionic chain packing.

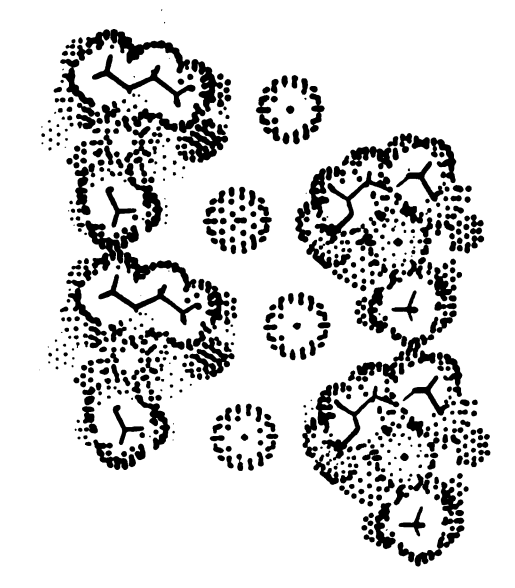


Figure 2-9. A thin section on the <u>b-c</u> plane of the  $Cs^+(C222).Cs^-$  structure showing the ionic chain packing.

8.97, 9.11 and 9.11 Å. The nearest Cs in an adjacent chain is at 10.03 Å.

4. Crystal structure of Rb<sup>+</sup>(C222).Rb<sup>-</sup>.

The Rb-C222 system has been studied for some time[15]. It was believed that there were two compounds: Rb<sup>+</sup>(C222).e<sup>-</sup> and Rb<sup>+</sup>(C222).Rb<sup>-</sup>. The existence of two compounds was implied by the EXAFS study [8,15], but there has not been reliable chemical analysis data to verify this. Solid state NMR experiments have failed to give any Rb<sup>-</sup> signal in the system. A preliminary experiment showed that the sample of "Rb<sup>+</sup>(C222).e<sup>-</sup>" had a rather high powder conductivity but no quantitative DC conductivity data were obtained [15].

The original goal of this work was to determine the crystal structure of the proposed electride: Rb<sup>+</sup>(C222).e<sup>-</sup>. Therefore the crystalline material from a Rb-C222 (1:1 ratio) synthesis was used along with some excess complexant C222 in the recrystallization to ensure the formation of the electride. The recrystallization methods are given in the Table 2-1. Only a few well-formed black single crystals were obtained.

The crystal data are summarized in the Table 2-6. One should notice that the a and c values of the cell parameters are identical within the standard deviations. Every effort

Table 2-6. Crystal Data of Rb (C222).Rb

Crystal dimensions : 0.25 x 0.30 x 0.40 mm

Temperature : 218 K

Space group : triclinic, Pī

Cell paramaters : a=12.418(4), b=12.419(3), c=11.582(3) Å, alpha=106.36(2),

c=11.582(3) Å, alpha=106.36(2), beta=94.80(3), gamma=62.38(2),

v=1506.8(7) Å<sup>3</sup>, Z=2

Peak width at

half-height : 0.50 degree

Scan type : theta- 2theta

Scan rate : 4 degrees/min. (in 2theta)

Maximum 2 theta : 45 degrees

No. of refl.measured: 5210

No. of unique refl. : 3970

No. of refl. used

in refinement :  $1671 \text{ with Fo}^2 > 3.0 \text{ sigma(Fo}^2)$ 

Corrections : Lorentz-polarization

Linear decay (1.000 to 1.461

on I)

Reflection averaging

 $(R_{int}=0.066)$ 

Empirical absorption (0.59 to 1.00 on I)

Solution : Patterson method

## Table 2-6. (cont'd)

Hydrogen atoms : ride on carbon atoms

R : 0.061

R<sub>tu</sub> : 0.069

High peak in final

diff. map : 0.84(9) e/Å<sup>3</sup>

Esd of obs. of

unit weight : 2.86

Convergence,

largest shift : 0.13 sigma

has been made to describe the structure in a higher symmetry class unsuccessfully.

An unexpected result was that the crystal structure data showed that the compound was a rubidide rather than an electride. In this compound, the distance between Rb and the closest H atom is 4.2 Å and the average distance of a Rb to the closest 14 atoms (all H atoms) is 4.4 Å. These give a minimum radius of 3.0 Å and an effective radius of 3.2 Å for the Rb anion. A striking feature of the structure is that the rubidium anions form pairs in the crystal. The distance between two paired rubidium anions is only 5.1 Å which is 1.3 Å shorter than the diameter of Rb (6.4 Å). The distance of an Rb ion in a pair to the nearest Rb in an adjacent pair is 7.9 Å. These results suggested a dimertype structure. Figure 2-10 clearly shows the nature of the "dimer" in this rubidide.

Alkali dimers in the gas phase have been known for a long time [21,22]. They are stable because the two selectrons are in the bonding orbital. The dissociation energies are in the range of 0.5 to 1.0 eV for  $Cs_2$  to  $Li_2$ . The observation of anionic dimers ( with two negative charges ) of alkali metals, however, has not been reported. No theoretical calculation data are available, but a zeroth order picture would predict no bonding. There are two electrons in the antibonding orbital in the dimer  $Rb_2^{2-}$ ; it

may not be stable and it is possible that it loses an electron from this antibonding orbital to become more stable. This may explain the rather high conductivity of the compound. The diamagnetic nature of the compound would require rather strong interactions between the electrons, however.

Although the overall structure of Rb<sup>+</sup>(C222).Rb<sup>-</sup> is quite different from that of K<sup>+</sup>(C222).e<sup>-</sup> ( monoclinic, C2/c ), the packings in both structures are similar. In Rb<sup>+</sup>(C222).Rb<sup>-</sup>, complexed cations form the same type of hexagonal patterns in the <u>a-b</u> plane as in K<sup>+</sup>(C222).e<sup>-</sup>. The cavities for the Rb<sup>2-</sup><sub>2</sub> dimers are also similar to those for the electron pairs in K<sup>+</sup>(C222).e ( Figure 2-10 and Figure 2-3 ). Figure 2-11 shows the hexagonal packing patterns in Rb<sup>+</sup>(C222).Rb<sup>-</sup>. Most of the properties of Rb<sup>+</sup>(C222).Rb<sup>-</sup> are still unknown, mainly because there may be an electride Rb<sup>+</sup>(C222).e<sup>-</sup> mixed with the rubidide, thus making the measurements more difficult to interpret. Low temperature powder x-ray crystallography should help us to understand this system.

5. Crystal structure of K<sup>+</sup>(C222).Na<sup>-</sup>.

As was mentioned before, the structure of  $K^+$  (C222).e<sup>-</sup> featured an electron pairing which was quite different from

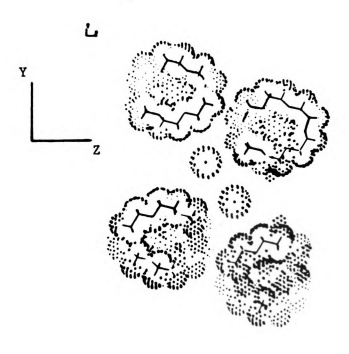


Figure 2-10. A thin section on the <u>b-c</u> plane of the  ${\rm Rb}^+({\rm C222}).{\rm Rb}^-$  structure showing the formation of the dimer  ${\rm Rb}_2^{2-}$ .

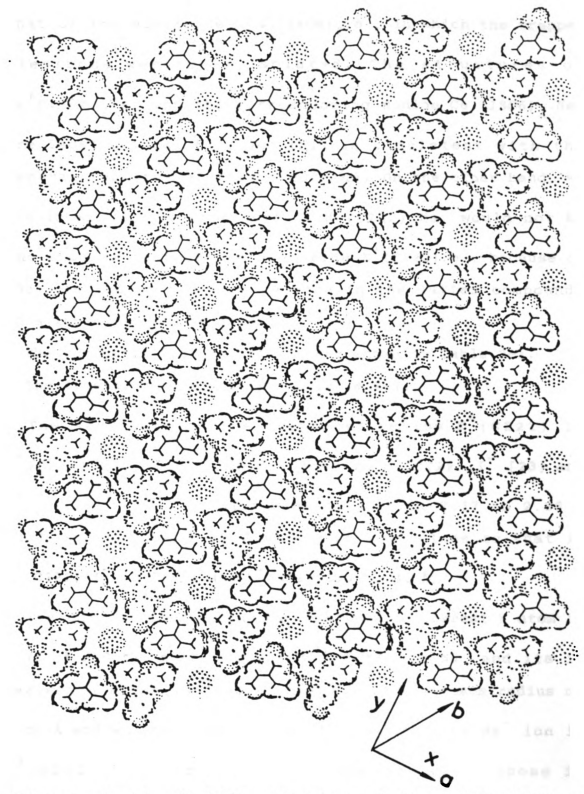


Figure 2-11. A thin section of the structure of  $Rb^{+}(C222).Rb^{-}$  in the <u>a-b</u> plane showing the hexagonal-type packing patterns similar to those in  $K^{+}(C222).e^{-}$ .

that of the electride,  $Cs^+(18C6)_2.e^-$ , in which the trapped electrons were well isolated. The structures of  $Cs^+(18C6)_2.e^-$  and the corresponding sodide  $Cs^+(18C6)_2.Na^-$  are isostructural [6] and this is consistent with the general features of this electride. On the other hand, we predicted that the structure of  $K^+(C222).Na^-$  would not be the same as that of the electride  $K^+(C222).e^-$ , because of the presence of electron pairing in the latter compound. This turned out to be true.

The recrystallization methods are shown in Table 2-1.

The crystal data are shown in Table 2-7.

The structure of the cryptated cation  $K^+(C222)$  in  $K^+(C222).Na^-$  is similar to those in  $K^+(C222).I^-$  [23] and  $K^+(C222).e^-$ . The  $K^+-0$  distances range from 2.77 to 2.86 Å with an average 2.82 Å which is very close to that in  $K^+(C222).I^-$  (2.79 Å) and  $K^+(C222).e^-$  (2.83 Å).

The distance between an Na ion and its nearest H atom is 3.75 Å and the average distance between the Na and its 14 nearest H atoms is 3.93 Å. These give a minimum radius of 2.55 Å and an effective radius of 2.73 Å for the Na ion in  $K^+(C222).Na$ . These figures are close to those in  $Cs^+(18C6)_2.Na$  (2.47 and 2.65 Å)[7] and  $Rb^+(15C5)_2.Na$  (2.60 and 2.99 Å)[8].

Table 2-7. Crystal Data of K+(C222).Na

Crystal dimensions : 0.4 x 0.5 x 0.8 mm

Temperature : 206 K

Space group : orthorhombic, Fdd2

Cell paramaters : a=15.769(7), b=25.245(7),

c=13.818(13) Å, V=5501(3) Å<sup>3</sup>, Z=8

Peak width at

half-height : 0.90 degree

Scan type : theta - 2theta

Scan rate : 2 degrees/min. (in 2theta)

Maximum 2 theta : 50 degrees

No. of refl.measured: 2764

No. of unique refl. : 1275

No. of refl. used

in refinement :  $1198 \text{ with Fo}^2 > 3.0 \text{ (Fo}^2)$ 

Corrections : Lorentz-polarization

Linear decay (0.972 to 1.526

on I)

Reflection averaging (R<sub>int</sub>=1.2%)

Numerical absorption (0.889 to 0.928 on I)

Extinction

 $(coefficient = 1.28 \times 10^{-7})$ 

Solution : Patterson method

## Table 2-7. (cont'd)

Hydrogen atoms : Located and refined isotropically

R : 0.021

R<sub>w</sub> : 0.021

High peak in final

diff. map :  $0.03(1) e/Å^3$ 

Low peak in final

diff. map :  $-0.02(1) e/\text{\AA}^3$ 

Esd of obs. of

unit weight : 0.38

Convergence,

largest shift : 0.10 sigma

The packing of the cations and anions is rather simple: all cations are in special positions and the cations and anions pack alternately along the <u>c</u>-axis. Each anion Na is coordinated by six cations at the distances of 5.736, 7.783, 7.783, 7.971, 7.971 and 8.082 Å, and vice versa for each cation. The shortest Na -Na and  $K^+-K^+$  distances are 8.204 Å.

# 6. Crystal structure of Cs<sup>+</sup>(15C5)<sub>2</sub>.K<sup>-</sup>.

Several potasside compounds have been synthesized and studied [24]. The structure of  $\mathrm{Cs}^+(15\mathrm{C5})_2.\mathrm{K}^-$  is the first crystal structure of a potasside.

Potassides are known to be difficult to handle and easy to decompose. It took several attempts to get good quality single crystals. The recrystallization conditions are shown in Table 2-1. The crystal data are given in Table 2-8. Its structure is very similar to that of  $Rb^+(15C5)_2.Na^-$  ( C2/m, a=11.555, b=13.587, c=9.958 Å, beta=92.03 degree, V=1562.4 Å<sup>3</sup>, z=2)[8,19].

Only one half of the crown ether (15C5) is crystallographically unique. Both cations and anions are in special positions. The crown atom C8 ( see the molecular diagram ) was found to be disordered and was refined as two half-occupancy atoms C8a and C8b.

Table 2-8. Crystal Data of Cs<sup>+</sup>(15C5)<sub>2</sub>.K<sup>-</sup>

Crystal dimensions : 0.2 x 0.4 x 0.9 mm

Temperature : 213 K

Space group : monoclinic, C2/m

Cell paramaters :

a=11.537(4), b=13.679(3), c=10.624(3) Å, beta=90.12(2),

V=1676.6(8)  $A^3$ , Z=2

Peak width at

half-height : 0.40 degree

Scan type theta-2theta :

Scan rate 2 degrees/min (in 2theta)

60 degrees Maximum 2 theta :

No. of refl.measured : 4345

No. of unique refl. : 1570

No. of refl. used

: 1453 with Fo<sup>2</sup> > 3.0 sigma(Fo<sup>2</sup>) in refinement

Corrections Lorentz-polarization

Linear decay

(0.996 to 1.317 on I)

Reflection averaging (R<sub>int</sub>=2.3%)

Numerical absorption (0.404 to 0.812 on I)

Solution : direct methods

## Table 2-8. (cont'd.)

Hydrogen atoms : located and refined isotropically

R : 0.067

R<sub>w</sub> : 0.075

High peak in final

diff. map :  $0.72(6) e/Å^3$ 

Low peak in final

**diff.** map :  $-0.57(6) e/Å^3$ 

Esd of obs. of

unit weight : 1.459

Convergence,

largest shift : 0.13 sigma

The cations and anions each form planes parallel to the <u>ab</u> plane respectively and the two types of planes alternate along the <u>c</u>-axis with intervals of 5.32 Å (  $1/2 \text{ of } \underline{c}$  ). Each cation is coordinated by 8 anions at distances of 7.859, 7.885, 7.885, 8.686, 8.686, 8.686 and 8.686 Å and vice versa for anions. The shortest  $K^--K^-$  and  $Cs^+-Cs^+$  distances are 8.985 Å. Therefore the anions are well isolated from each other. The  $^{39}K$  solid state NMR spectrum of this compound showed a  $K^-$  peak at -105 ppm from  $K^+$ (aq.) [24].

The distance between a  $K^-$  and its nearest H atom is 3.97 Å and the average of the 16 shortest  $K^-$ H distances is 4.34 Å. These values yield a minimum radius of 2.8 Å and an effective radius of 3.15 Å for  $K^-$ .

#### CHAPTER 3

### PHOTOEMISSION OF ALKALIDES AND ELECTRIDES

### 3.1 Background.

In the last two decades photoelectron spectroscopy ( PES ) has been developed into a powerful technique for studying electronic structures in gases [28,29], liquids [30] and solids [31,32] and has been widely used in solid state physics [31,32] ( especially semiconductor physics ), surface science [32], chemical analysis [33,34] and other related fields.

Photoelectron emission (photoemission) was discovered in 1887 by Hertz [36] when he was studying the nature of sparking phenomena. The puzzling facts that photoemission happened only under certain color lights for certain materials and that the photoemission intensity depended on the intensity of light was resolved by Einstein in 1905 [37] in terms of the simple relationship:

$$E_{kin.max} = h \nu - \emptyset \qquad (3.1)$$

i.e. the maximum kinetic energy  $E_{\rm kin}$  of a photoelectron is equal to a quantized package of light energy  $h\nu$  minus the "work function"  $\phi$  which is related to the emitter. This equation remains to date the most fundamental relationship in photoemission and forms the basis of the single-(independent) electron approximation. Figure 3-1 shows the Einstein relation.

Photoemission is actually a complicated, many-body process. This problem can not be solved without making approximations. The single-electron approximation assumes that the incident photon interacts with a single electron and the total energy of the photon is absorbed by the electron. Then the Einstein equation can be rewritten in more complete form as:

$$E_{kin} = h\nu - \phi - E_{i} \qquad (3.2)$$

where E<sub>i</sub> is the energy of the electron, i.e. the ionization energy. We see the photoemission process as one in which a photon excites an electron from an occupied state (initial state) to an empty state (final state). The number of possible transitions is proportional to the number of available states in both energy levels. That is, the photoemission spectra reflect the product of the densities of the initial and final states.

$$n(E) = N_{C}(E) \times N_{V}(E-h\nu) \qquad (3.3)$$

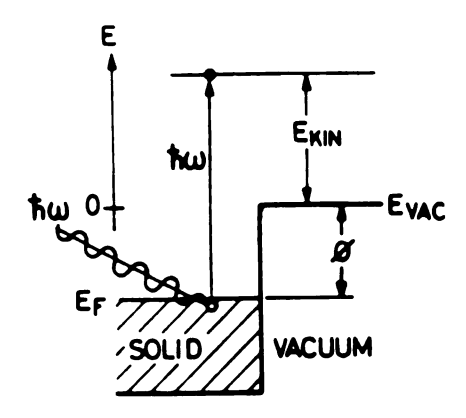


Figure 3-1. Photoexcitation of electrons from a solid by photons of energy  $\hbar\omega$ .  $\phi$  is the workfunction,  $E_{\rm vac}$  is the energy of the vacuum level,  $E_{\rm kin}$  is the kinetic energy of emitted electrons,  $E_{\rm F}$  is the Fermi energy.

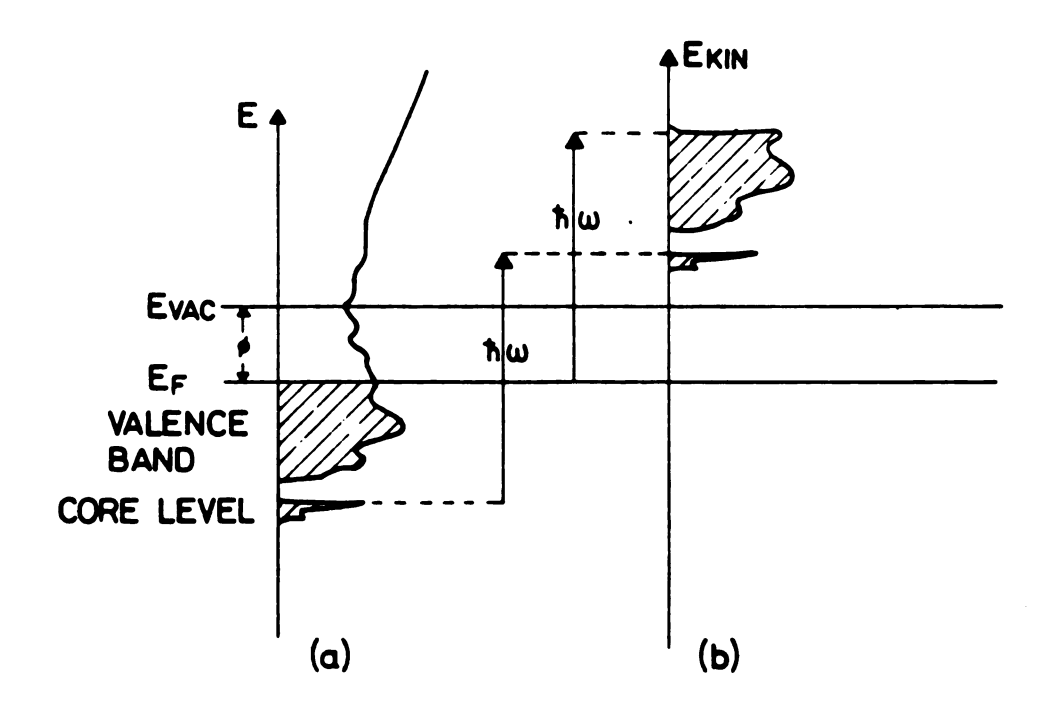


Figure 3-2. Illustration of the fact that the density of electronic states distribution of the emitter, part (a), is reflected in the photoemission spectral fine structure, part (b). [ref.32].

n(E) is the number of electrons excited to the energy E,  $N_{C}(E) \text{ and } N_{V}(E-h\nu) \text{ are the densities of states at the final state energy E and the initial state energy <math>E-h\nu$  respectively.

We assume further that the final state is a free electron state in the vacuum for which the density of states is rather flat. We may then take the density of final states as a constant.

Under these assumptions we rewrite the equation (3.3)

$$n(E) = N_v(E-h\nu) \qquad (3.4)$$

i.e. the photoemission spectra map out the density profile of the initial states which is the information about energy states that we want to know. This is illustrated in Figure 3-2.

Beyond the approximation mentioned above we have to consider a number of points. First, the final state may be a state of the excited electron in the bulk which is not equivalent to a state in the vacuum continuum. The excited electron may suffer from scattering ( electron-electron or electron-phonon scattering, elastic or inelastic ) before it reaches the surface. Scattering causes broadening of the photoemission peaks or the appearance of energy-loss peaks on the low kinetic energy side of the true photoemission peaks. Second, the final states and initial states can show strong spatial variation ( particularly in the surface region ) which forms the basis for the study of the angular

distribution spectrum of photoemission. Third, the optical excitation can be a many-body process and the initial states may include the states of some other electrons. These effects are manifested in the so-called shake-up and shake-off processes [34,35].

With all these effects to complicate the process, photoemission would seem to be uninterpretable in terms of the known electronic energy levels in solids. This, however, is not true. Not all of the above possible contributions occur at the same time or with the same weight. In fact, the simple density of states model works remarkably well for most experimental spectra.

Photoemission is a process that involves both surface and volume effects, and therefore can provide information on surface as well as bulk electronic structures. The surface sensitivity of photoemission is determined by the fact that, although the usual light beam can penetrate far into solids (on the order of several tens of atomic layers, hundreds of Å), photoelectrons that are excited by light suffer from electron-electron and/or electron-phonon collisions in solids and thus the mean free path is very limited. Figure 3-3 shows the relationship of the mean free path to the kinetic energy of photoelectrons. In the region of a few eV to 1000 eV the mean free path is only a few tens of angstroms. Therefore, the surface condition is extremely important in photoemission. This is why the development and application of quantitative photoemission methods had been

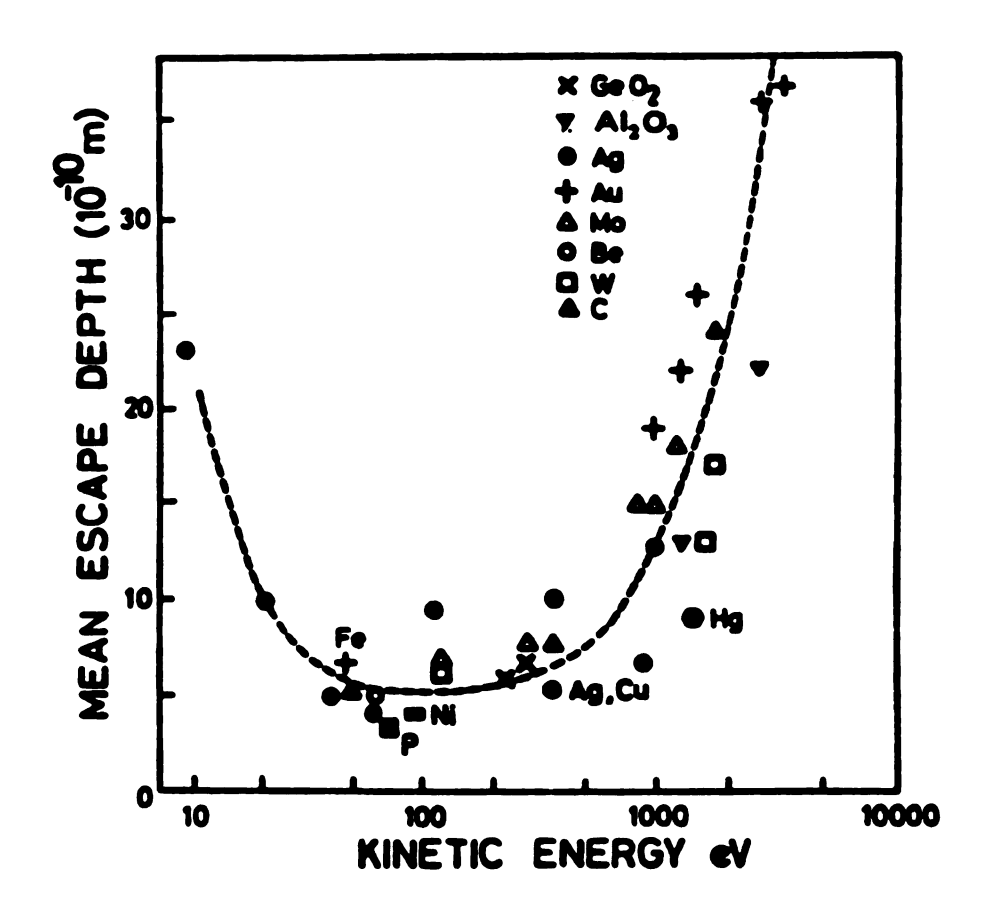


Figure 3-3. Energy dependence of the escape depth of excited electrons showing the mean free path as a function of kinetic energy. [Ref.34]

hampered by poor vacuum techniques until the 60's when ultra high vacuum (UHV) was available. It is known that under a vacuum of  $10^{-5}$  to  $10^{-6}$  torr, a monolayer of molecules of vapor gas will be deposited onto a clean surface in less than a second. But it will take hours if the vacuum is  $10^{-10}$  torr. Only under UHV or the complete absence of reactive gases can accurate, reproducible PES data from solids be obtained.

The power of PES over other methods of studying the electronic structures in solids, such as optical absorption or reflection spectroscopy is the following: First, an optical spectrum integrates over all possible excitations for which energy conservation holds, while in PES the final states are known ( the states in vacuum continuum with energy  $\mathbf{E}_{kin}$ ). Only the initial states which fit the Einstein equation are responsible for the spectrum. Second, PES resolves the final state energy of the excited electron directly and thus permits the determination of absolute energies, while an optical spectrum determines the difference of levels only.

There are two major measurements in PES: energy distribution curves (EDC), and quantum yield spectra.

EDC is most often used. It is obtained by measuring the intensities of photoelectrons with different kinetic energies while the energy of the photon is fixed. Figure 3-2 shows the principle behind EDC.

A quantum yield spectrum is made by measuring the total photoemission current under a potential which is high enough to collect all photoelectrons while the wavelength of the light is scanned. It is an integral measurement over all photoemission electrons. Usually a quantum yield spectrum is used to determine the work function of a solid by extrapolating the quantum yield curve to zero yield. Figure 3-4 shows a quantum yield spectrum of copper.

Some previous work had been done on the relative quantum yield spectra of some sodides in our laboratory [10]. The photoemission cell shown in Figure 3-5 was used. A small ion pump was used to maintain a vacuum of better than 10<sup>-4</sup> Torr. The sodide films were made on a platinum electrode by dissolving sodide crystals in methylamine and then evaporating the solvent. The photoemission quantum yields from the films of four sodides were similar with one peak at 370 nm and another at about 600 nm. The yields were strongly temperature-dependent and the reason was not known. The two peaks were assigned to trapped electrons (600 nm) and sodide anions (370 nm).

The present studies continued the work on photoemission. A new apparatus was built and experiments on other alkalides and electrides as well as on sodides were carried out.

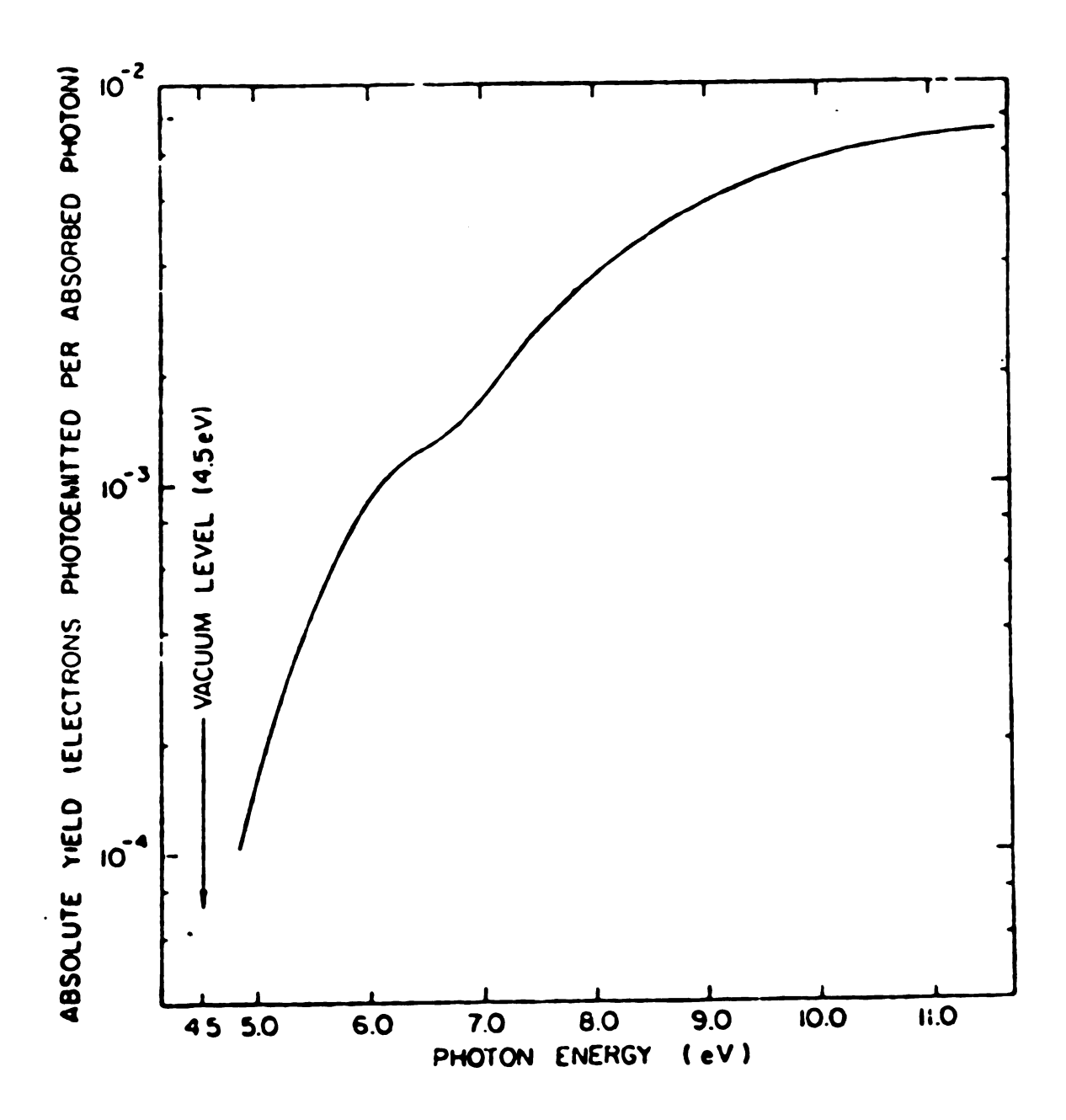


Figure 3-4. Quantum yield spectrum of a clean copper surface. [Ref.42]

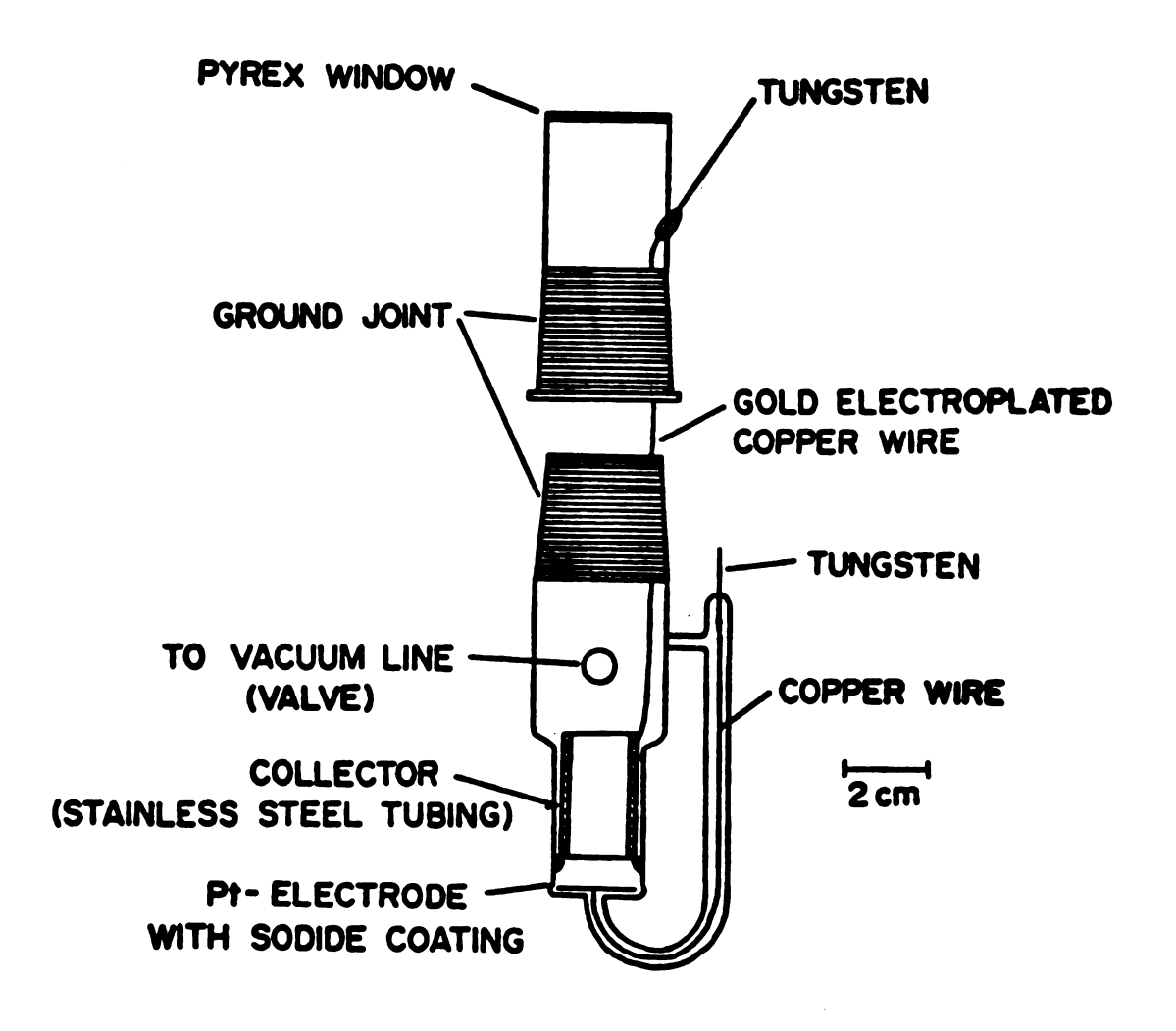


Figure 3-5. Photoemission cell for studying the photoemission of sodides. [Ref.10]

#### 3.2 Experimental.

# 3.2.1 Experimental system.

The experimental set-up is shown diagrammatically in Figure 3-6. The system consists of the following parts:

#### A. Photoemission chamber.

The spherical retarding potential analyzer consists of an emitter, grid and collector ( anode ). The emitter is cooled with cold nitrogen gas. The whole cathode unit except the sample holder on its top is enclosed in a vacuum jacket to keep its outside surface warm while the sample holder is cold. This avoids solvent condensation on the probe during the film making process. The grid is made from stainless steel and has a diameter of 2 inches. The potential on the grid can be controlled for different purposes. Usually the grid is at the cathode potential during EDC measurements in order to form a field-free region for photoemission. In quantum yield experiments, however, the grid is connected to the collector in order to sweep all emitted electrons from the region of the cathode. The spherical collector is made of brass and has a 4" diameter. It is isolated from the ground by Teflon.

The vacuum chamber is made from stainless steel with a quartz window on its top to allow the light beam to come in.

The chamber is also the housing for the preamplifier.

#### B. Optical system.

# Photoemission Apparatus

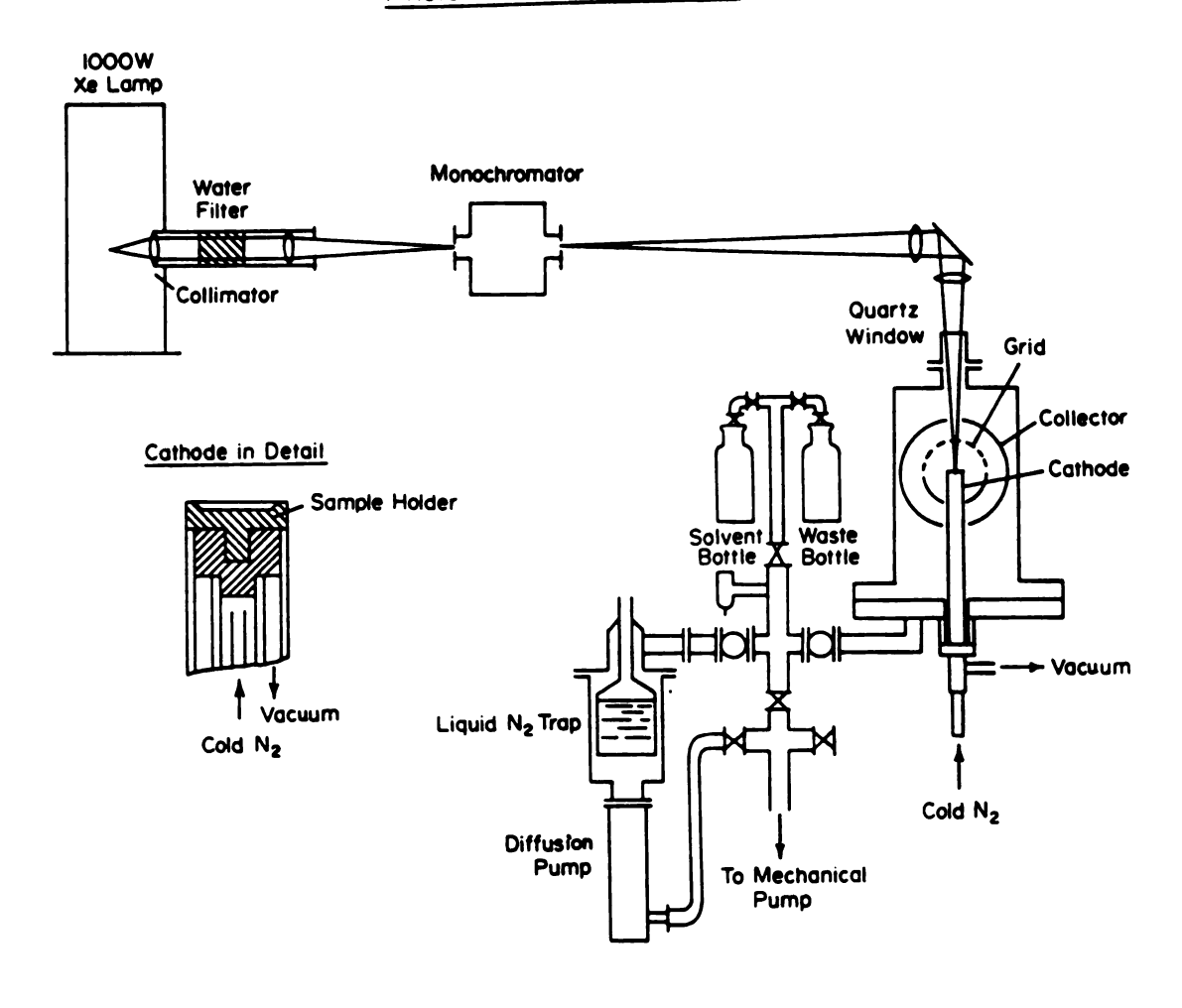


Figure 3-6. Photoemission experimental system used in this work.

A 1000 watt Xe-lamp serves as the light source. After passing through a water filter ( not used when IR light is needed. ) and an Oriel 77250 monochromator, the light beam is collimated and focussed on the sample holder.

#### C. Vacuum system.

The vacuum system consists of a liquid nitrogen trap, a diffusion pump and a mechanical pump. Usually the vacuum is between  $5x10^{-6}$  and  $1x10^{-5}$  torr.

# D. Solvent system.

In order to make films on the holder, some solvent is used. Usually MeNH<sub>2</sub> or Me<sub>2</sub>O is used. A solvent bottle and a waste bottle are connected to the vacuum chamber.

### E. Electronic system.

The electronic system consists of a preamplifier, a main amplifier and an x-y recorder. The sensitivity of the electronic system is about one picoampere.

#### 3.2.2 Experimental procedure.

#### A. Film making.

After the mechanical and then the diffusion pump are turned on, liquid nitrogen is poured into the trap. The vacuum should then be at about  $1-2\times10^{-5}$  torr. The valve between the trap and the manifold is closed and house nitrogen is introduced into the chamber to bring the pressure to atmospheric. The emitter probe is lowered from the chamber onto a support. Nitrogen gas, cooled by liquid

nitrogen in a dewar, passes through the probe, and the temperature of the holder ( -100 to -50 °C ) is controlled by regulating the flow . The crystalline sample is then put on the holder. When strong static electricity tends to make the crystals fly off the holder, one or two drops of cold pentane are added to the crystals to keep them in the cathode cup. The probe is inserted back into the chamber and the chamber is evacuated. During the whole experiment, cold nitrogen gas is used to keep the sample holder at the desired temperature. When the vacuum in the chamber reaches  $1x10^{-5}$  torr or lower, the valve between the trap and the manifold is closed and solvent vapor is introduced into the chamber and condenses on the holder. The crystals dissolve and a blue solution can be seen through the quartz window. Then the solvent is evaporated by opening the valve to the waste bottle which is kept in liquid nitrogen. In this way, a fresh solvent-free film is deposited on the holder.

#### B. Quantum yield measurement.

A potential high enough to collect all photoelectrons (usually 5-10 V) is applied to the collector and the grid. The photocurrent is converted into a voltage signal by the preamplifier and the main amplifier and is recorded by an x-y recorder where the time base mode is used for the wavelength scan. While the wavelength is being scanned, the photocurrent is recorded. The photon flux was measured by a UV detector ( 1 cm $^2$  area, model UV-444 BQ from EG & G, calibrated by EG & G. ). The quantum yield was calculated

without making a reflection correction. Therefore the calculated quantum yields are lower than the actual values.

C. EDC measurement. The potential on the grid is set to the ground. The wavelength is fixed at a certain value. The retarding potential is scanned and is input into the x mode of the recorder. The photocurrent is recorded by the y mode.

#### 3.3 Results and discussion.

Attempts to measure energy distribution curves were unsuccessful. Whenever the retarding potential was set to zero, the photocurrent was zero. The reason is obvious, however : a space charge built up on the film which prevented the electron from escaping from the surface. This problem is common when semiconductor films are used. It could also be seen that as soon as a fresh film was made the color changed from golden or red to gray in seconds. This might indicate that surface contamination is a serious problem that could be the major source of the space charge. Alternatively, the color change could result from the formation of a finely divided polycrystalline film as the last traces of solvent were removed. Because of these problems only photoemission quantum yields are reported in this work. The reproducibility obtained suggests that such measurements may not be as sensitive to surface contamination as are EDC studies.

The following sodides, potassides and electrides were tested first by the quantum yield experiment: Na<sup>+</sup>(C222).Na<sup>-</sup>,

K<sup>+</sup>(15C5)<sub>2</sub>.Na<sup>-</sup>, K<sup>+</sup>(15C5)<sub>2</sub>.K<sup>-</sup>, K<sup>+</sup>(15C5)<sub>2</sub>.e, Cs<sup>+</sup>(18C6)<sub>2</sub>.Na<sup>-</sup>, Cs<sup>+</sup>(18C6)<sub>2</sub>.e. While Na<sup>+</sup>(C222).Na<sup>-</sup>, Cs<sup>+</sup>(18C6)<sub>2</sub>.Na<sup>-</sup> and Cs<sup>+</sup>(18C6)<sub>2</sub>.e gave very low quantum yields. K<sup>+</sup>(15C5)<sub>2</sub>.Na, K<sup>+</sup>(15C5)<sub>2</sub>.K and K<sup>+</sup>(15C5)<sub>2</sub>.e showed high yields. Surprisingly, the spectra of these compounds with different anions Na<sup>-</sup>, K<sup>-</sup> and e were initially very similar. The quantum yield spectra showed a few peaks in the UV and visible region and the photoemission extended into the IR region up to about 1 micron but did not show any peaks in the region of 600 nm and longer wavelengths.

In addition to the previously observed peak at about 370 nm there were two other peaks in these compounds: 300 nm and 330 nm independent of the anions (Na, K or e). This was unexpected and caused us to abandon the method for a long time. We expected that different anions would give different peaks.

The origin of these uniform results was finally found. The key was Na contamination, apparently from Pyrex glass. All of the compounds used earlier in this work had been synthesized in Pyrex glass apparatus. It has been known for a long time that when Pyrex glassware comes in contact with a solution of alkali anions other than sodide, a rapid exchange process occurs:

$$M^- + Na^+(glass) \implies M^+ (glass) + Na^-$$

The exchange process reaches an equilibrium with a small amount of Na in the solution. This Na contamination was too small to affect most optical, NMR or other measurements. However it affects the photoemission spectrum very seriously because photoemission is very sensitive to the surface. When a film is made the major compound (containing Kor e) may have crystallized first and the Na last so that the concentration of Na in the surface layer may be much higher than the average value. Figure 3-7 shows the marked effect of Na contamination.

The photoemission quantum yield spectrum of K<sup>+</sup>(15C5)<sub>2</sub>K<sup>-</sup> which was synthesized in a quartz cell is shown in Figure 3-8. It is clear that the peak at 370 nm is from K<sup>-</sup>. There are two small shoulders at 300 and 330 nm which could be from a small amount of Na contamination. This is strongly suggested by the photoemission spectrum of Na<sup>+</sup>(C222).Na<sup>-</sup> shown in Figure 3-9. The Na contamination may be from a trace of Na in the K metal or from the glassware used in the K metal distribution or distillation.

Figure 3-10 shows the spectrum of  $Rb^+(15C5)_2$ .  $Rb^-$  in which there is a new peak at 380 nm in addition to the peaks at the same location as those of  $K^-$  and  $Na^-$ ( 370, 330, 300 nm). The new peak is assigned to  $Rb^-$ . The major peaks of  $K^-$ 

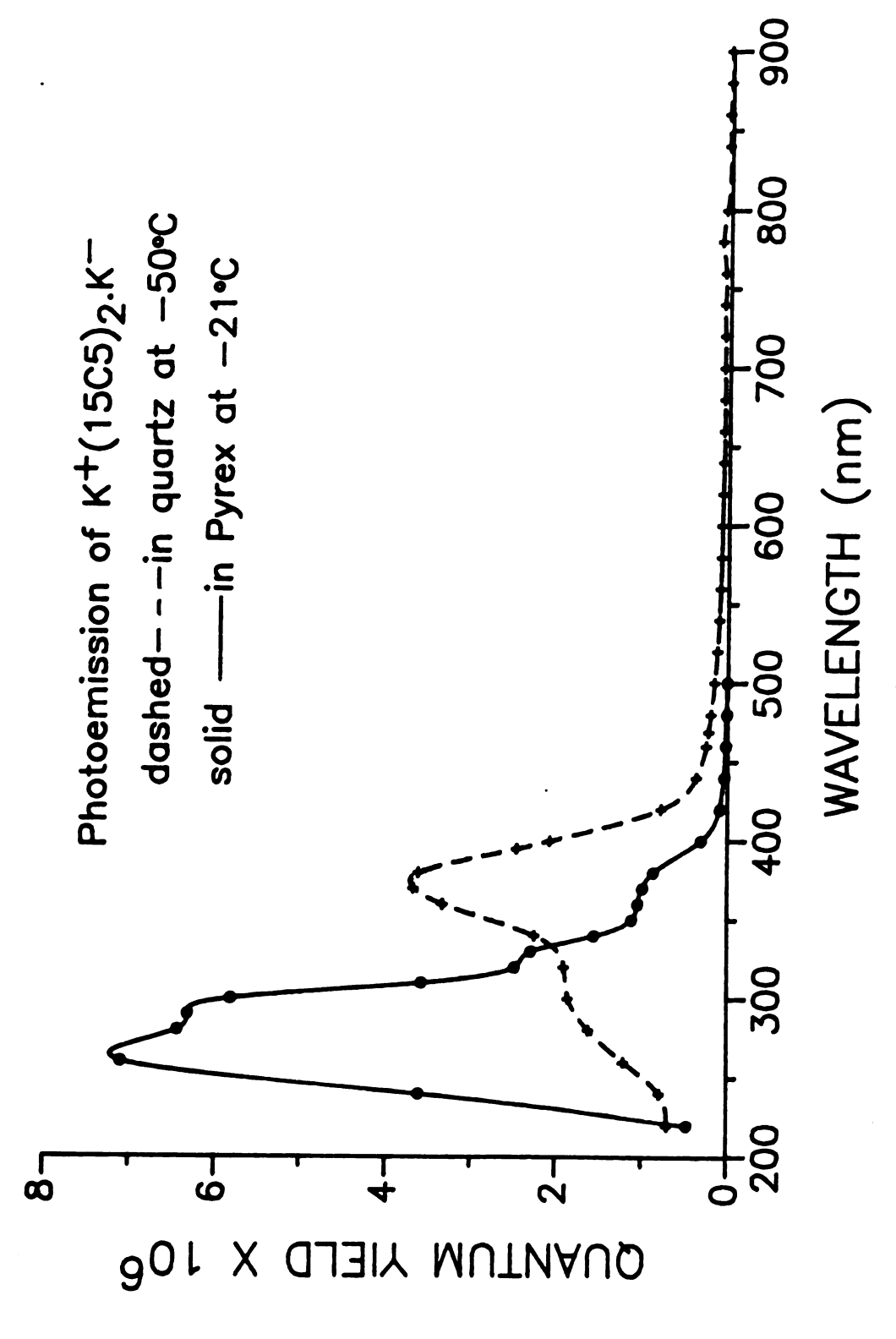
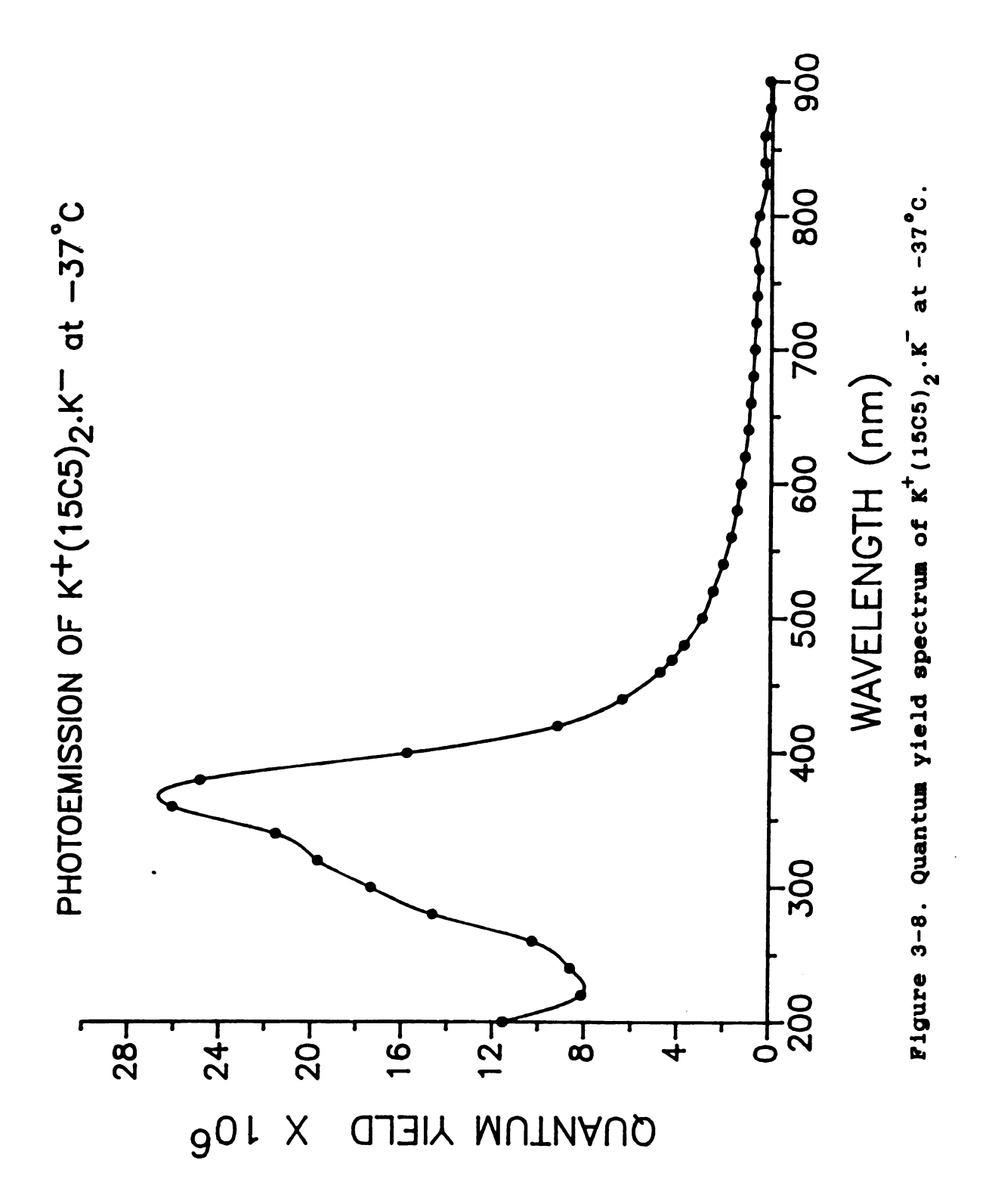
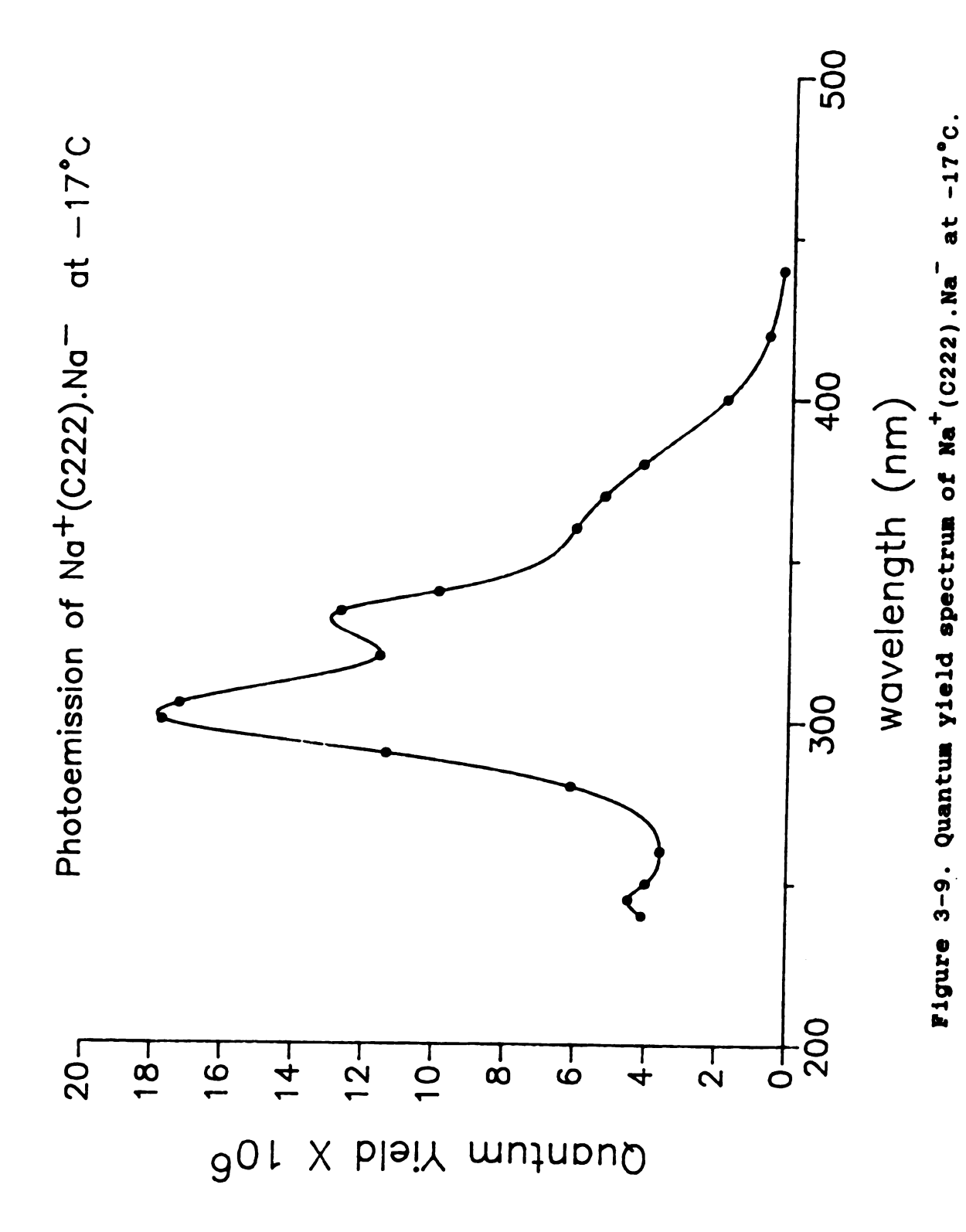


Figure 3-7. Quantum yield spectra of  $\mathtt{K}^+(15C5)_2.\mathtt{K}^-$  showing the effect of Na contamination. Solid curve, synthesized in a Pyrex cell. Dashed curve, synthesized in a quartz cell.





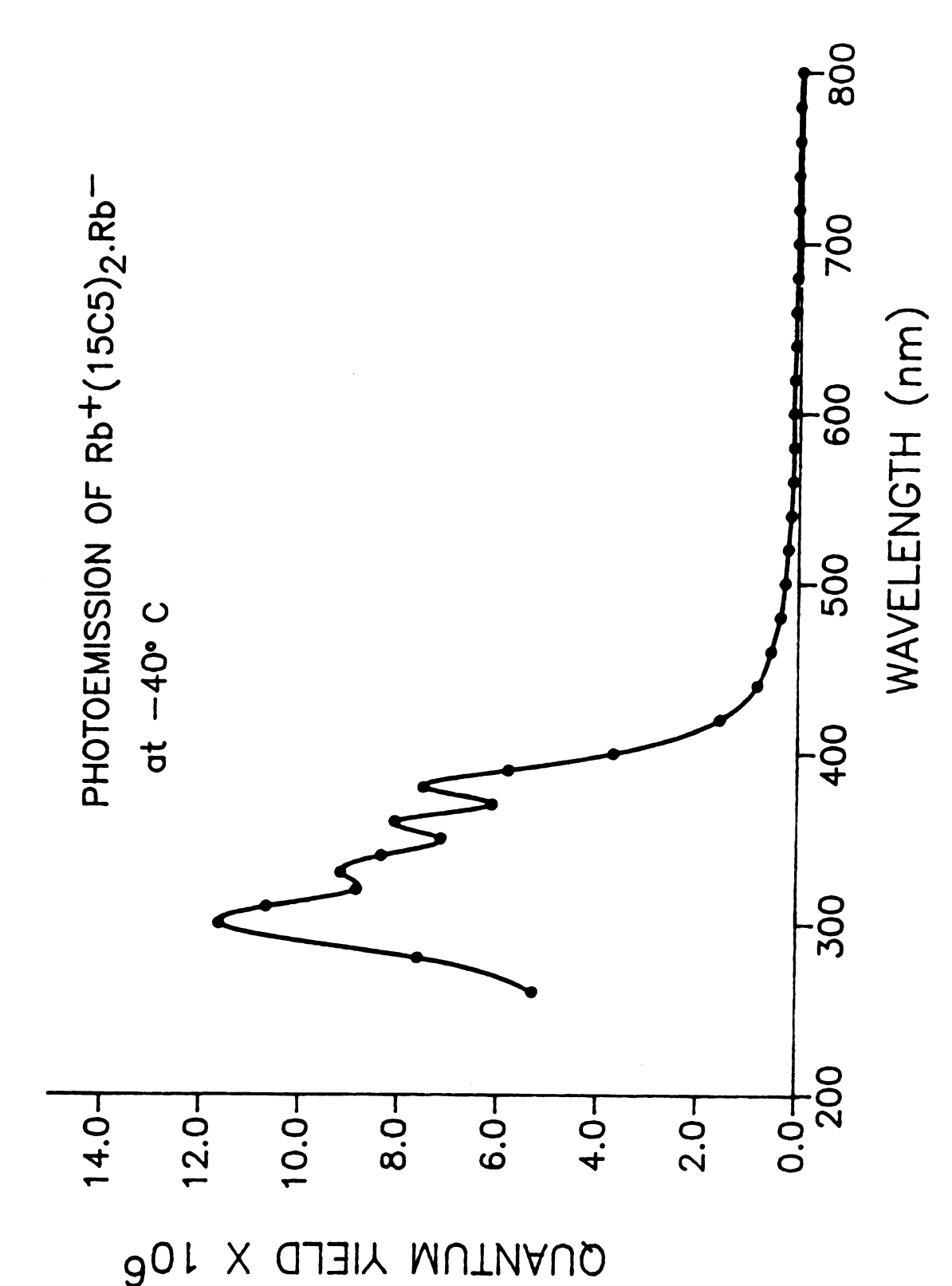
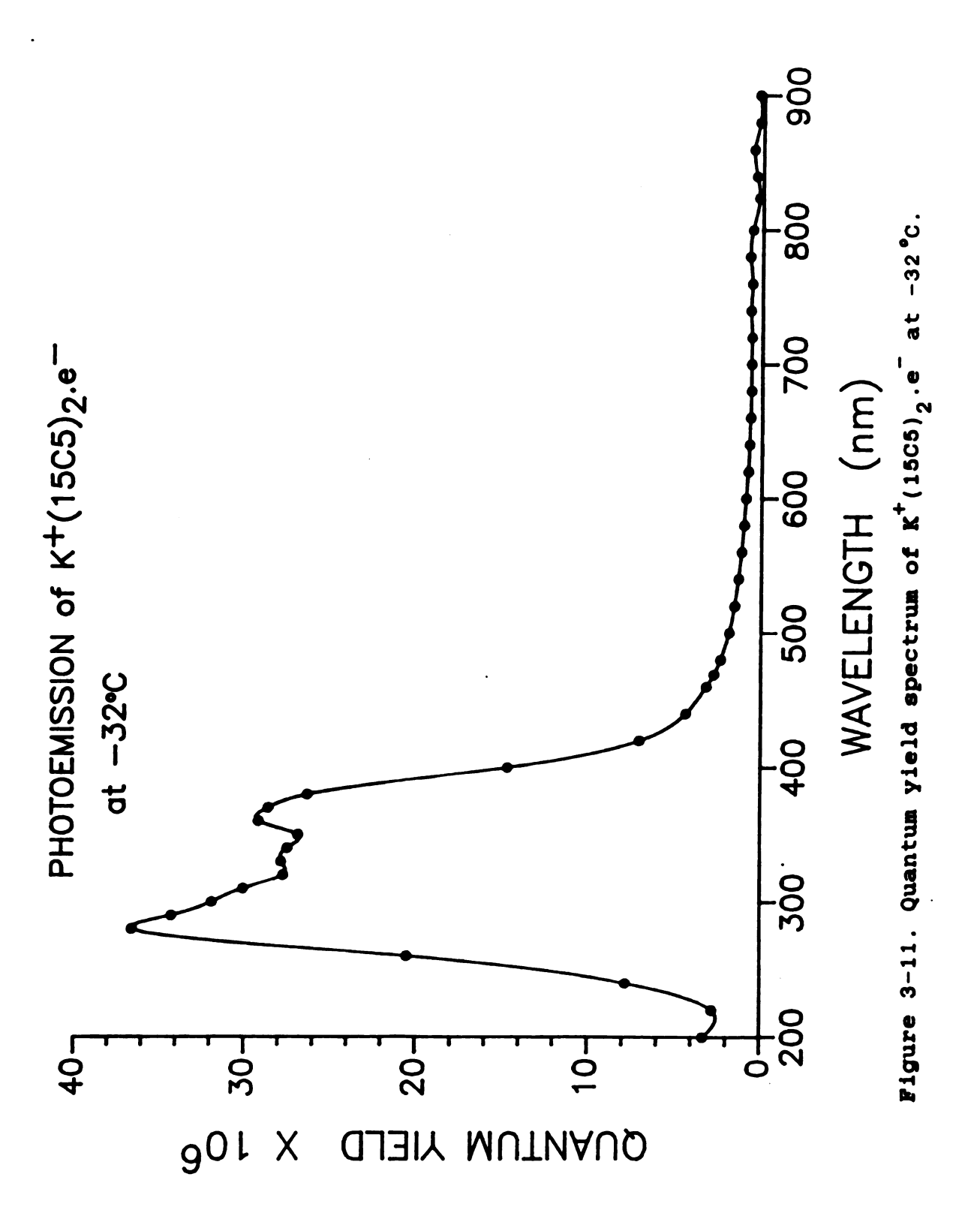


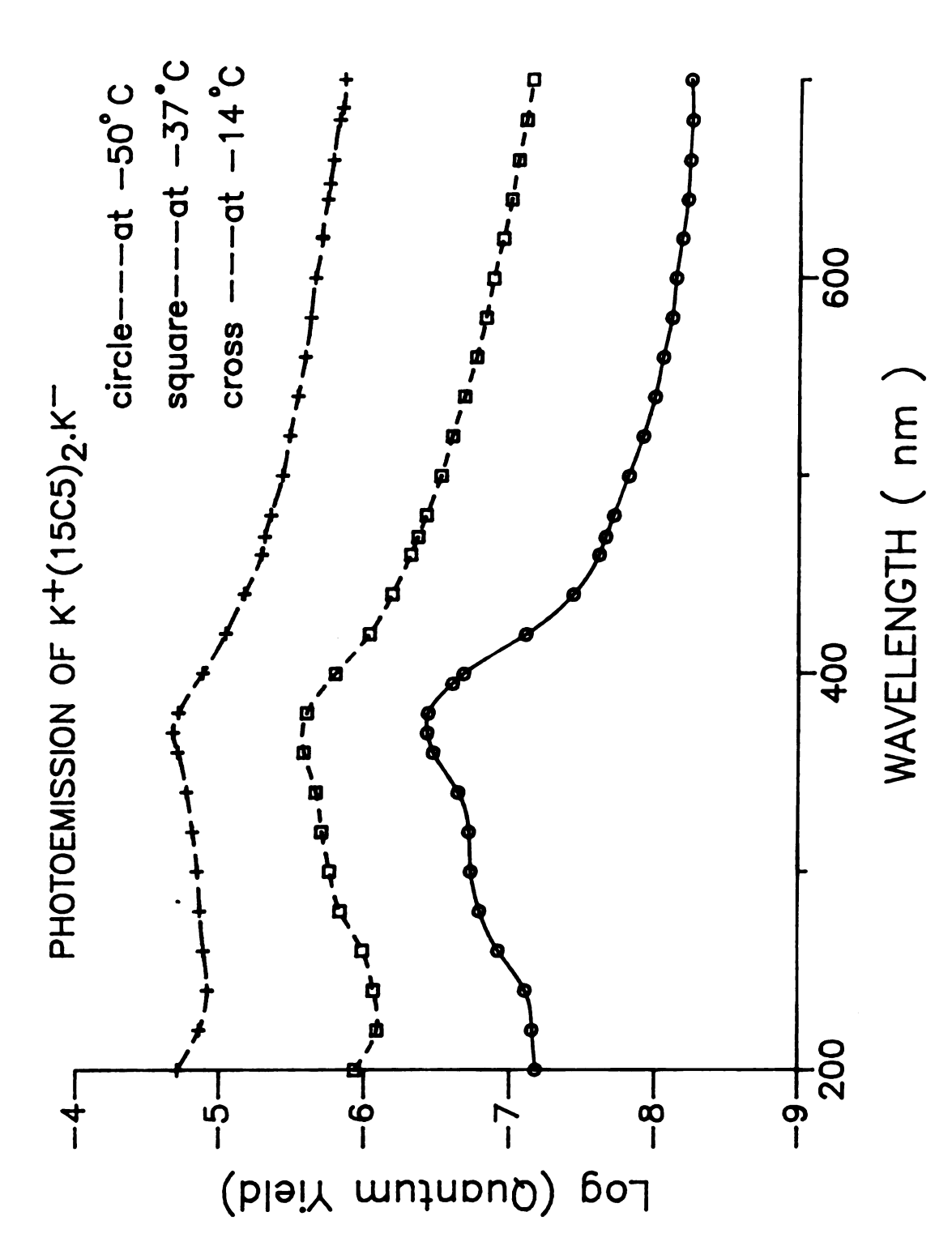
Figure 3-10. Quantum yield spectrum of Rb (15C5)2.Rb at -40°C.

and Rb are very close, consistent with the optical absorption results.

What is/are responsible for the photoemission in the low energy region is still not clear. It is believed to be from trapped electrons. However the emission from an electride film did not give a substantially higher yield at low energies. Figure 3-11 shows the quantum yield spectrum of a film of  $K^+(15C5)_2$ .e. The signal does not seem to be much higher than that from  $K^+$ (15C5)<sub>2</sub>. $K^-$ . However, we should remember that there is always some electride K+ (15C5)2.emixed with the potasside and some K in the electride. The photoemission spectrum of K<sup>+</sup>(15C5)<sub>2</sub>.K<sup>-</sup> may have some contribution from the electride, and vice versa. We must consider the complication that different phases are formed from different compounds ( electride and alkalide ) in a thin film. The phase with the higher quantum yield will then dominate the spectrum.

All photoemission spectra showed a strong temperature dependence. Figure 3-12 shows the temperature dependence of the quantum yield of  $K^+(15C5)_2.K^-$ . The mechanism behind it is still not clear. Surface contamination resulting in an insulating layer on the surface may be responsible. Alternatively, the photoemission mechanism may involve a thermal activation step. In order to eliminate the effects





Figuer 3-12. Temperature dependence of the quantum yield of  $K^{\dagger}$  (15C5)  $_2$  .  $K^{-}$  .

of surface contamination it will be necessary to construct a system that will allow us to obtain better vacuum conditions.

Alkalides and electrides are, we believe, some of the most difficult materials to handle in photoemission studies due to their high reactivities with air and/or moisture and the sensitivities to heat. Although the surface contamination was a serious problem and EDC measurements were unsuccessful, the quantum yield measurements were surprisingly reproducible. The shifts of peaks for Na, K or Rb in different runs with the same or different cations were within the experimental errors ( a few nm ), therefore these peaks are real. The in situ film making technique used in this work ensures that the films are fresh. It is certainly much better than the preformed film technique which we have tried before. The use of ultra high vacuum technique and/or modern photoemission apparatus should help us to overcome the surface contamination problems.

#### CHAPTER 4

#### Thermionic Emission from Alkalides and Electrides

When a metal is heated to a high temperature, the electrons in the conduction band may gain enough energy to overcome the work function barrier and escape from the metal surface into a vacuum. This is the well-known thermionic emission phenomena. From the Boltzmann distribution, the number of electrons with energy E is

$$N = N_0 \exp (-E/kT) \qquad (4.1)$$

 $N_{\Omega}$  being the total number of electrons in the ground states.

It is clear that only when kT is comparable to E will there be a significant number of electrons which are able to escape. At room temperature, kT is about 0.025 eV. The work functions of normal metals are higher than 2 eV, so there is no thermionic emission from normal metals at room temperature. The work functions of common semiconductors ( defined as the energy difference between the Fermi energy and the vacuum continuum ) are usually at least a few eV.

In alkalides and electrides, however, the valence electrons are either weakly bound (in alkalides) or trapped in the lattice (electrides). The cations are well shielded by the big cryptand or crown ether molecules. Therefore we should expect the work functions to be lower than those of normal semiconductors.

Thermionic emission was reported from solvated electrons in Na-hexamethylphosphoric triamide solution by Delahay [30] and by Gremmo and Randles [41]. This thermionic emission was seen at room temperature and the temperature dependence of the thermoemission current yielded an activation energy of about 1 eV.

Thermionic emission from alkalides and electrides was first seen with a sample of K<sup>+</sup>(15C5)<sub>2</sub>.K<sup>-</sup> during a photoemission experiment. After a fresh film had been made by MeNH<sub>2</sub> evaporation, the potential between the anode and the cathode yielded a high current signal without any light illumination at low temperatures ( about -60°C ). Figure 4-1 shows the current signal during MeNH<sub>2</sub> evaporation. It can be seen that either when the film was still wet or the film was fresh, the thermionic emission signal was high ( a few nA ) and then decreased with time and stabilized at a few pA.

Thermionic emission has now been observed from crystals of alkalides and electrides as well as from films formed by solvent evaporation. After the crystalline alkalides or electrides were loaded onto the sample holder and covered

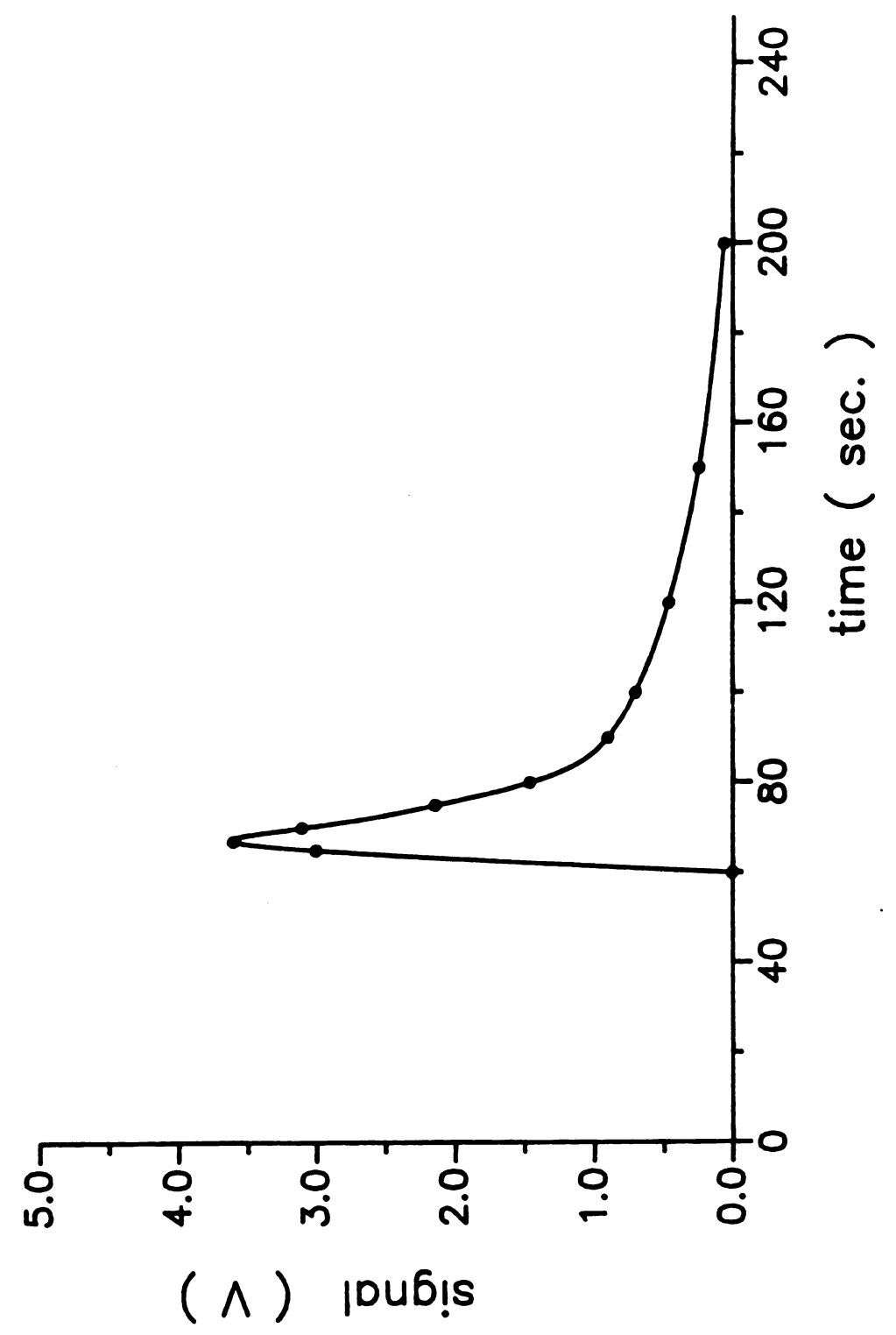


Figure 4-1. Thermionic emission current signal during film making of  $K^+(15C5)_2$ . $K^-$ . MeNH<sub>2</sub> was used as solvent. The temperature was about -60 °C.

with pentane ( to avoid static electricity ) and then inserted into the vacuum chamber, the pentane was pumped out and a current signal appeared ( a few nA ). The signal stayed at a few pA for a long time ( a few hours ) at temperatures around -60 °C.

The thermionic emission current depended on the temperature and the potential between the emitter and the collector. The current- potential curve reached saturation at relatively low potentials. In our case, the saturation potential was only a few volts. Figure 4-2 shows the saturation curve for a film of Rb<sup>+</sup>(15C5)<sub>2</sub>.Rb<sup>-</sup>. The saturation potential was about 5 V.

The temperature dependence follows the Richardson-Dushman equation:

$$j = A (1-r)T^{2} \exp(-e\phi/kT) \qquad (4.2)$$

j is the current density, T is the temperature, A is a constant related to elementary physical constants, r is the reflection coefficient for electrons. This equation was derived from a thermodynamic method that involved the use of Clapeyron's equation under the assumption that the electron gas in gas phase is in equilibrium with the hot conductor and obeys the laws for an ideal gas[39,40]. Assuming that A, r and  $\phi$  are independent of temperature, one can find the work function  $\phi$  by plotting  $\ln (j/T^2)$  versus 1/T (Richardson plot ). Preliminary results showed work

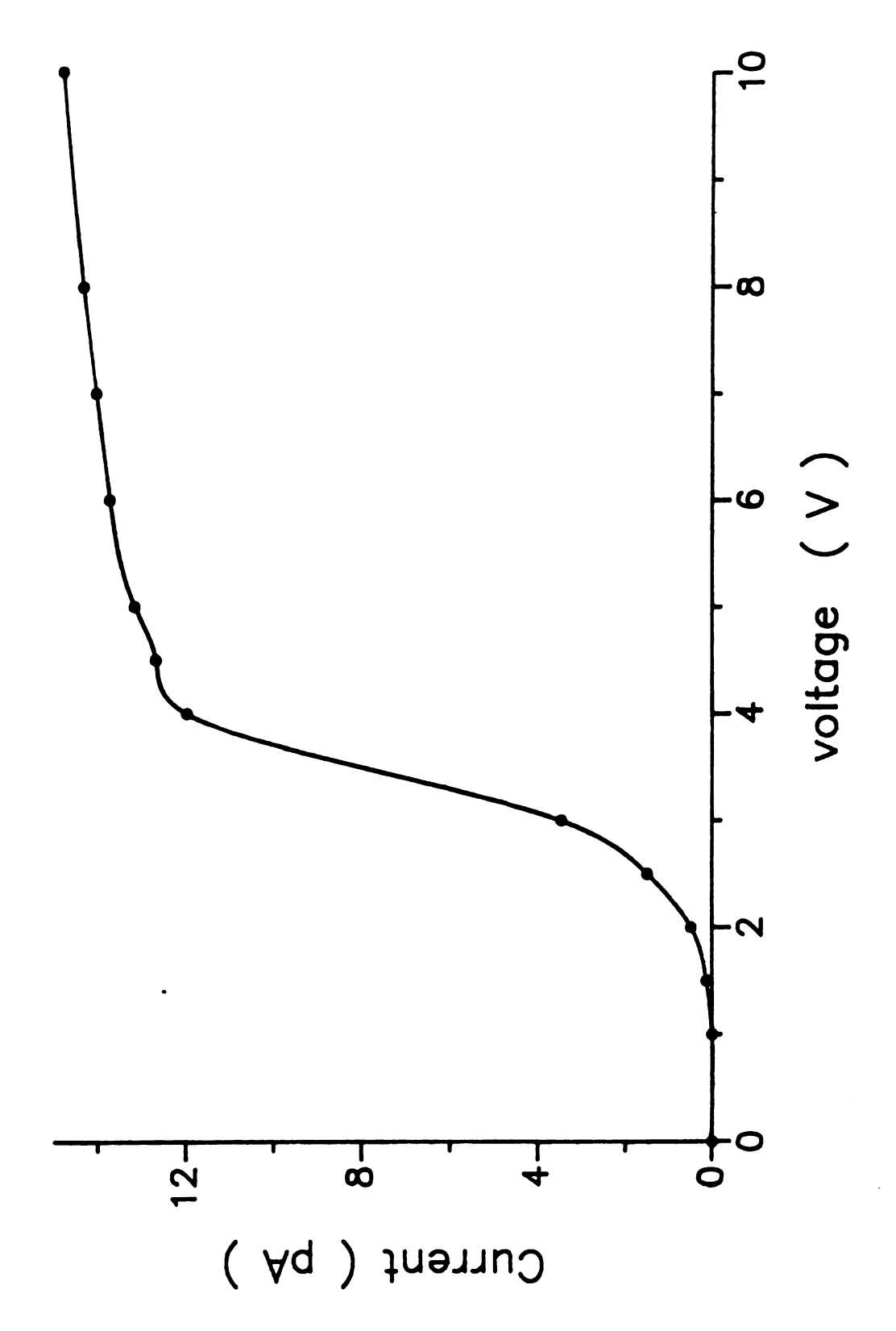
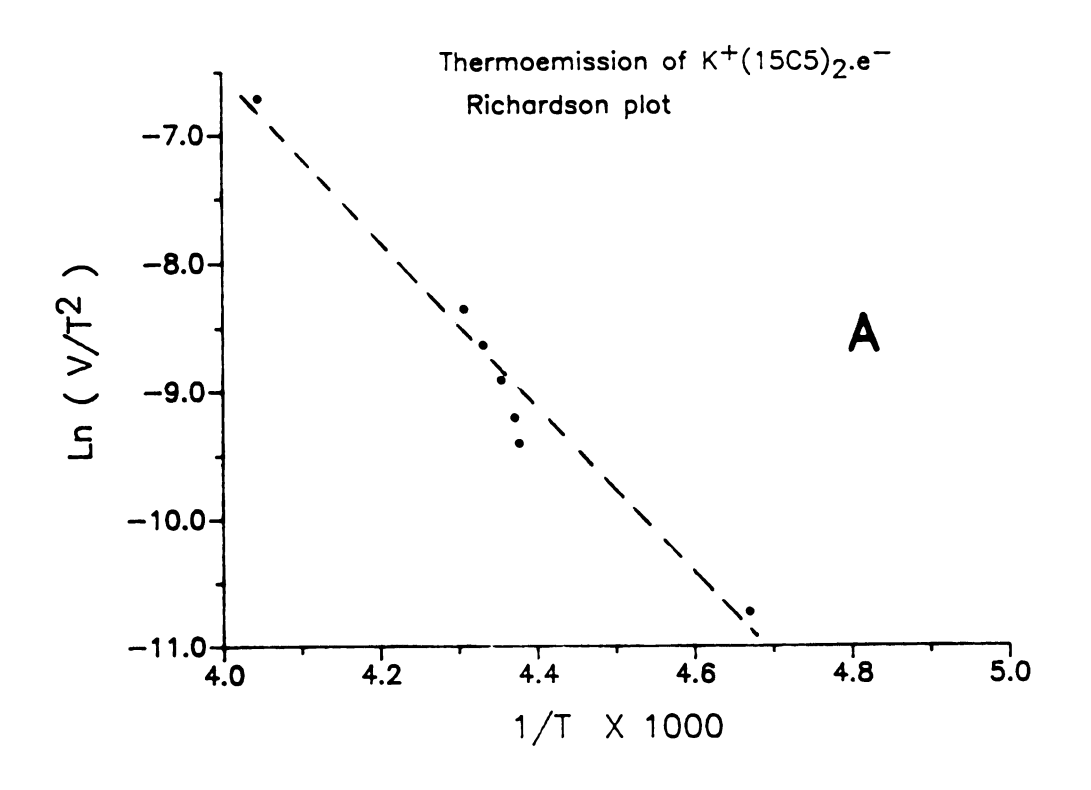


Figure 4-2. Saturation curve of the thermionic emission current for a film of Rb<sup>+</sup>(15C5)<sub>2</sub>.Rb<sup>-</sup> at -30°C.

functions that ranged from 0.2 eV to 0.6 eV as shown in Figure 4-3.

The work function is a many-body phenomena. This problem can not be solved exactly. However the problem is conceptually simple: a finite piece of the solid is considered and its ground state energy  $\mathbf{E}_{\mathbf{N}}$  is calculated in the neutral state with N electrons. A calculation is performed for the state of charge +1, with only N-1 electrons, and the corresponding ground state energy  $\mathbf{E}_{\mathbf{N}=\mathbf{1}}$  is obtained. The difference  $\mathbf{E_{N}} - \mathbf{E_{N-1}}$  is taken as the work function . Surface, of course, plays the major role in the work function. Sometimes one assumes that the surface is made of whole cells with the same shape and same charge distribution as in the bulk. But a real surface actually does not have the same charge distribution as the bulk. Sometimes electrons tend to "spill out" of the surface plane so as to decrease their kinetic energy. And sometimes a smoothing out of the rough charge distribution due to crevices between Wigner-Seitz cells at the surface takes place[31]. Figure 4-4 shows the "spill out" and "smooth out" processes. In the case of "spill out", a surface charge layer is introduced and tends to increase the work function. On the other hand, smoothing processes tend to decrease the work function.

Therefore we have



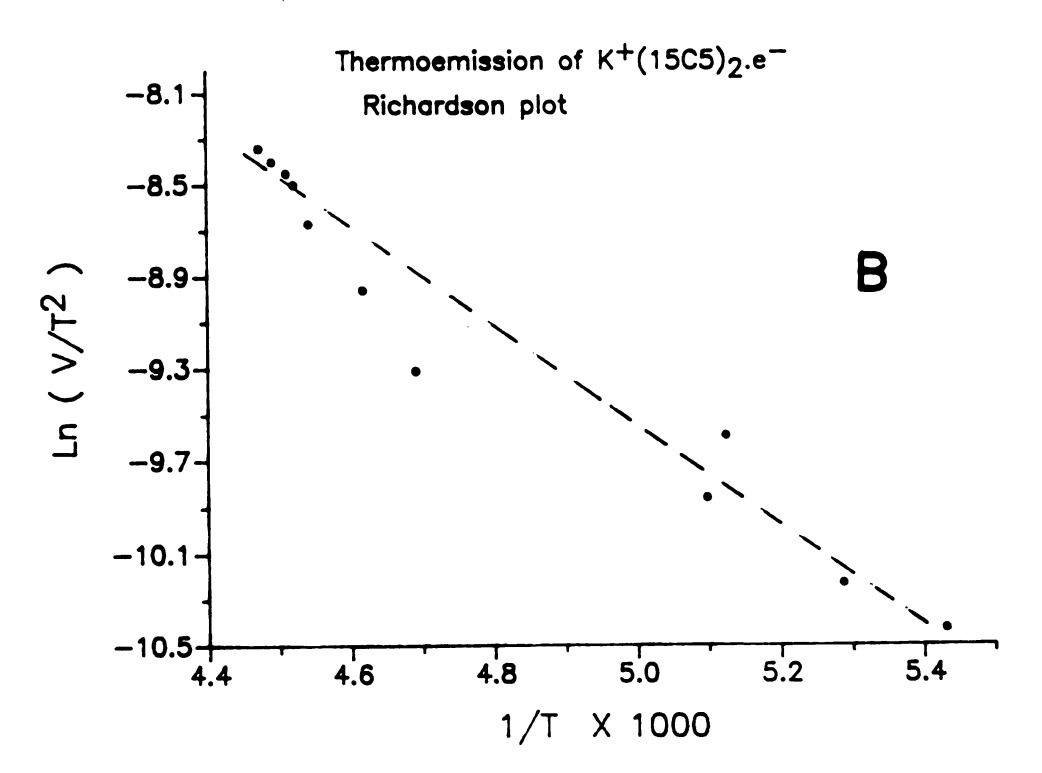
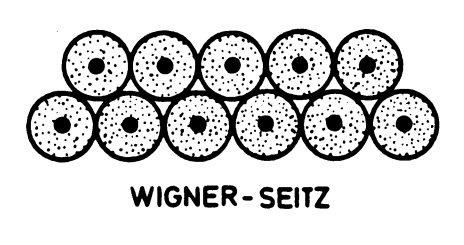


Figure 4-3. Richardson plot of the thermionic emission of  $K^+(15C5)_2.e^-$  from film (A) and crystals (B).





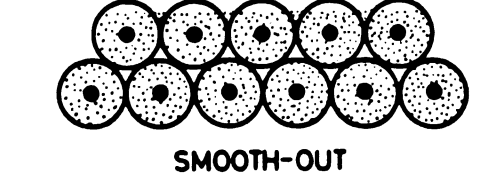


Figure 4-4. Diagram showing the electron distribution in the Wigner-Seitz spheres and the effects of electron spill-out and smooth-out near a surface. [Ref.31]

$$\Phi = -\mu + D \tag{4.3}$$

where  $E_N - E_{N-1} = -\mu$ , the so-called internal work function,  $\mu$  is the electrochemical potential and D is the total double layer dipole from the "spill out" and/or smoothing.

For alkalides and electrides, valence electrons are either weakly bound (in alkalides) or trapped (electrides). The contribution from the electrochemical potential is expected to be small. The contribution of D depends on the electron density near the surface and the tightness of packing. Since the complexed cations and alkalide anions are all large species and the cations are well-shielded by the cryptand or crown ether molecules, the electron density is low and the packing is loose near the surface. This makes the contribution of D to the work function small. Overall we should expect low work functions for these compounds.

Unfortunately the vacuum in our system was not good enough to keep the films clean and surface contamination was a serious problem.

Nevertheless, thermionic emission at temperatures as low as 200 K has not been previously reported and this is certainly the lowest thermionic emission temperature observed from any solid. Work functions as low as 0.5 eV are the lowest for any solid and suggest numerous applications for electrides.

#### CHAPTER 5

# SUMMARY AND CONCLUSIONS

1. The crystal structures of one electride and five alkalides have been determined. The crystal structure of  $K^{+}(C222).e^{-}$  provides the structural evidence for electron pairing, consistent with other properties of this electride. A minimum radius of 3.1 Å and an effective radius of 3.5 Å have been obtained from the structures of Cs + (18C6)2.Cs and Cs + (C222).Cs -. The cesium anions form chains in both structures. The cesium anions in Cs + (18C6) 2.Cs are wellisolated from each other, while the anions in Cs<sup>+</sup>(C222).Cs<sup>-</sup> are in contact with each other. The structures provide the explanation for the presence of a Cs solid state NMR peak in Cs<sup>+</sup>(18C6)<sub>2</sub>.Cs<sup>-</sup> and the absence in Cs<sup>+</sup>(C222).Cs<sup>-</sup>. The anions in  $Rb^+(C222).Rb^-$  form dimer-type species  $Rb_2^{2-}$ . The minimum and effective radii obtained from these structures are: 3.0 and 3.2 Å for Rb, 2.8 and 3.15 Å for K and 2.55 and 2.73 Å for Na.

- 2. Photoemission from some sodides, potassides, rubidides and electrides has been studied. Sodium contamination from Pyrex glassware has a great effect on the photoemission quantum yield spectra of the electrides and alkalides other than sodides. The photoemission peaks for the alkali metal anions are: 300 and 330 nm for Na, 370 nm for K and 380 nm for Rb. In most of the cases the photoemission extends into the IR region ( about 1 micron ). The quantum yields are strongly temperature dependent.
- 3. Thermionic emission has been observed from the crystals and films of alkalides and electrides at temperatures as low as -60 °C. Fresh or wet films ( or crystals ) show high emission currents. The temperature dependence of the thermionic emission current follows the Richardson-Dushman equation and the Richardson plots of the films and crystals of alkalides and electrides yield work functions of a few tenths of an eV.



#### APPENDIX 1.

Crystal structure data of  $K^+(C222).Na^-$ ,  $Cs^+(18C6)_2.Cs^-$ ,  $Cs^+(C222).Cs^-$ ,  $Rb^+(C222).Rb^-$ ,  $K^+(C222).Na^-$  and  $Cs^+(15C5)_2.K^-$ .

This appendix collects some major structural data for each of these compounds. These data are the following:

- 1. drawing of single molecule.
- 2. stereoview of unit cell.
- table of positional parameters and their estimated standard deviations.
- 4. table of bond distances.

For those structures in which the H-atoms ride on the carbon atoms to which they belong, the parameters related to H-atoms are not included.

Table A-1

Table of Positional Parameters and Their Estimated Standard Deviations for Potassium Cryptand [2.2.2] Electride

Atom	<b>x</b> -	<u>Y</u>	<b>z</b> <del>-</del>	B(Å <sup>2</sup> )
K1 O4 O7 O13 O16 O21 O24 N10 C23 C5 C6 C8 C9 C112 C12 C12 C15 C18 C19 C22 C22 C22 C22 C22 C22 C22 C2	0.75630(4) 0.8032(2) 0.8697(2) 0.5596(1) 0.5516(1) 0.8879(1) 0.8695(2) 0.7364(2) 0.7759(2) 0.7343(2) 0.8205(2) 0.8767(2) 0.8512(2) 0.8543(3) 0.8624(3) 0.6691(3) 0.5712(3) 0.4735(2) 0.4546(2) 0.5338(2) 0.6332(2) 0.6332(2) 0.6332(2) 0.8318(2) 0.6332(2) 0.9254(2) 0.9610(2) 0.9254(2) 0.9610(2) 0.9254(2) 0.965(2) 0.8990(3) 0.8048(3) 0.745(2) 0.894(2) 0.894(2) 0.951(2) 0.864(2) 0.778(2)	0.08333(3) -0.03005(9) -0.0209(1) 0.0827(1) 0.11103(9) 0.16757(8) 0.1868(1) 0.0833(1) 0.0831(2) 0.0165(2) -0.0266(1) -0.0752(2) -0.0805(2) -0.0805(2) -0.0805(2) 0.0980(2) 0.0980(2) 0.1199(1) 0.0980(1) 0.1168(2) 0.1180(2) 0.1180(2) 0.1180(2) 0.1800(1) 0.2245(1) 0.2245(1) 0.2245(1) 0.187(2) 0.1487(2) 0.1487(2) 0.1487(2) 0.014(1) -0.068(1) -0.068(1) -0.012(1) -0.060(1) -0.118(1) -0.095(1)	0.04166(3) -0.0224(1) 0.1070(1) 0.10540(8) -0.02329(8) -0.02146(9) 0.10733(9) -0.0974(1) 0.1797(1) -0.1199(1) -0.0863(2) 0.0101(2) 0.0757(2) 0.1722(2) 0.2025(2) 0.2019(2) 0.1699(2) 0.0736(1) 0.079(1) -0.0880(1) -0.1203(1) -0.1203(1) -0.1197(1) -0.0858(1) 0.0109(2) 0.0771(2) 0.1724(2) 0.2025(2) -0.164(1) -0.114(1) -0.103(1) -0.103(1) -0.090(1) 0.005(1) -0.010(1) 0.081(1)	3.22(4) 4.99(5) 4.09(4) 3.34(4) 3.61(4) 4.57(5) 3.56(4) 5.07(7) 5.71(8) 6.89(9) 6.36(9) 6.36(9) 6.36(9) 6.36(6) 4.13(6) 4.13(6) 4.15(6) 4.42(7) 4.61(7) 6.6(1) 2.7(7) 2.7(7) 3.0(7) 3.2(7)
Н6b Н8а Н8b	0.893(2) 0.905(3) 0.785(3)	-0.111(1) -0.056(2) -0.049(2)	0.100(1) 0.192(2) 0.173(2)	2.8(7)* 5.1(9)* 5(1)*

#### Table A-1 (continued)

# Table of Positional Parameters and Their Estimated Standard Deviations for Potassium Cryptand [2.2.2] Electride

-----

Atom	x	v	Z	B(Å <sup>2</sup> )
7	_	<b>y</b>	_	
H9a	0.861(3)	0.031(2)	0.251(1)	3.6(8)*
н9Ь	0.936(2)	0.057(1)	0.195(1)	2.6(7)*
H11a	0.667(2)	0.071(2)	0.248(1)	3.9(8)*
H11b	0.658(3)	0.013(2)	0.197(2)	7(1)*
H12a	0.501(3)	0.084(2)	0.191(1)	4.3(8)*
H12b	0.573(3)	0.143(2)	0.176(1)	4.1(8)*
H14a	0.493(2)	0.167(1)	0.076(1)	1.5(6)*
H14b	0.406(2)	0.116(1)	0.096(1)	1.3(5)*
H15a	0.436(2)	0.053(1)	0.003(1)	1.0(5)*
H15b	0.394(2)	0.127(1)	-0.014(1)	1.3(5)*
H17a	0.472(2)	0.119(1)	-0.105(1)	0.7(5)*
H17b	0.514(2)	0.049(1)	-0.092(1)	1.0(5)*
H18a	0.617(2)	0.109(1)	-0.167(1)	2.7(7)*
H18b	0.644(2)	0.165(1)	-0.114(1)	1.6(6)*
H19a	0.819(2)	0.127(1)	-0.166(1)	1.4(6)*
H19b	0.894(2)	0.089(1)	-0.114(1)	1.7(6)*
H20a	0.921(2)	0.202(1)	-0.104(1)	1.7(6)*
H20b H22a	0.801(2)	0.212(1)	-0.092(1) 0.007(1)	1.2(5)* 2.1(6)*
	0.867(2) 0.984(2)	0.255(1) 0.242(1)	-0.009(1)	2.4(6)*
H22b H23a	1.017(2)	0.242(1)	0.080(1)	2.1(6)*
H23b	0.990(2)	0.1/3(1)	0.080(1)	2.4(6)*
H25a	0.923(3)	0.223(2)	0.192(2)	5.0(9)*
H25b	0.923(3)	0.151(2)	0.177(1)	3.5(8)*
H26a	0.824(3)	0.131(2)	0.251(2)	4.7(9)*
H26b	0.738(3)	0.179(2)	0.193(2)	4.4(8)*
11200	0.750(5)	0.17(2)	0.105(2)	414(0)

Starred atoms were refined isotropically.
Anisotropically refined atoms are given in the form of the isotropic equivalent thermal parameter defined as:

 $<sup>(4/3) * [</sup>a^2*B(1,1) + b^2*B(2,2) + c^2*B(3,3)$ 

<sup>+</sup>  $ab(\cos gamma)*B(1,2) + ac(\cos beta)*B(1,3)$ 

<sup>+</sup> bc(cos alpha)\*B(2,3)]

Table A-2

Table of Bond Distances (in Angstroms) for Potassium Cryptand [2.2.2] Electride

Atom1	Atom2	Distance
K1 K	O4 O7 O13 O16 O21 O24 N1 N10 C3 C5 C6 C8 C12 C15 C17 C22 C23 C25 C18 C19 C9 C11 C3 C6 C9 C12	2.805(2) 2.857(2) 2.858(2) 2.795(2) 2.798(2) 2.847(2) 2.981(2) 2.958(2) 1.412(4) 1.429(4) 1.429(4) 1.418(4) 1.422(3) 1.418(3) 1.428(3) 1.428(3) 1.428(3) 1.421(3) 1.421(4) 1.421(4) 1.464(4) 1.47(4) 1.464(4) 1.476(3) 1.479(4) 1.462(5) 1.483(4) 1.479(6) 1.477(6) 1.508(4) 1.477(6) 1.478(6) 1.507(5)
C14 C17 C19 C22 C25	C15 C18 C20 C23 C26	1.478(4) 1.508(4) 1.499(4) 1.483(5) 1.506(5)

Table A-2 (continued)

Table of Bond Distances (Continued) for Potassium Cryptand [2.2.2] Electride

C2 H2a 0.98(3) C2 H2b 0.95(3) C3 H3a 0.94(3) C3 H3b 0.95(3) C5 H5a 0.97(3) C5 H5b 0.99(3) C6 H6a 0.95(3) C6 H6b 0.94(3) C8 H8a 0.94(3) C8 H8b 0.96(4)	Atom1	Atom2	Distance
C3 H3a 0.94(3) C3 H3b 0.95(3) C5 H5a 0.97(3) C5 H5b 0.99(3) C6 H6a 0.95(3) C6 H6b 0.94(3) C8 H8a 0.94(3) C8 H8b 0.96(4)	C2		0.98(3)
C3 H3b 0.95(3) C5 H5a 0.97(3) C5 H5b 0.99(3) C6 H6a 0.95(3) C6 H6b 0.94(3) C8 H8a 0.94(3) C8 H8b 0.96(4)	C3		0.94(3)
C5 H5a 0.97(3) C5 H5b 0.99(3) C6 H6a 0.95(3) C6 H6b 0.94(3) C8 H8a 0.94(3) C8 H8b 0.96(4)	C3		
C5 H5b 0.99(3) C6 H6a 0.95(3) C6 H6b 0.94(3) C8 H8a 0.94(3) C8 H8b 0.96(4)	C5		
C6 H6a 0.95(3) C6 H6b 0.94(3) C8 H8a 0.94(3) C8 H8b 0.96(4)	C5		
C6 H6b 0.94(3) C8 H8a 0.94(3) C8 H8b 0.96(4)		нба	0.95(3)
C8 H8a 0.94(3) C8 H8b 0.96(4)		<b>H6</b> b	0.94(3)
			0.94(3)
CO HO2 1 06/31			
C) H3Q 1.00(3)	C9	H9a	1.06(3)
C9 H9b 1.01(3)			
C11 H11a 1.01(3)			
C11 H11b 1.04(4)	C11		
C12 H12a 1.03(3)	C12		
C12 H12b 0.93(3)	C12		
C14 H14a 1.00(3)	C14	H14a	
C14 H14b 0.99(3)		H14b	0.99(3)
C15 H15a 0.97(2)			0.97(2)
C15 H15b 1.01(2)			
C17 H17a 0.94(2)			
C17 H17b 1.01(2)			
C18 H18a 1.02(3)	C18		1.02(3)
C18 H18b 1.01(3)	C18		
C19 H19a 1.01(3)	C19	H19a	
C19 H19b 0.96(3) C20 H20a 0.99(3)	C19	H13D	0.96(3)
	C20	HZUA HZON	0.99(3)
C20 H20b 0.98(2) C22 H22a 0.95(3)		H20D	0.90(2)
C22 H22b 0.93(3)			
C23 H23a 0.97(3)			
C23 H23b 0.97(3)			
$\begin{array}{cccccccccccccccccccccccccccccccccccc$	C25		
C25 H25b 0.96(3)	C25		
C26 H26a 1.04(3)	C26	H26a	
C26 H26b 1.02(3)			

Numbers in parentheses are estimated standard deviations in the least significant digits.

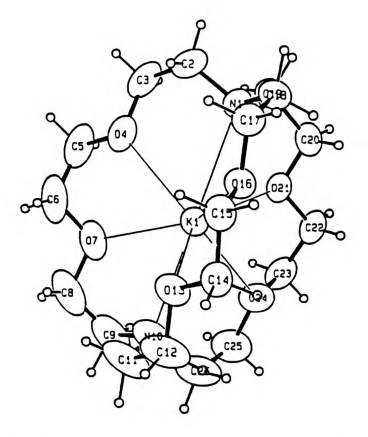


Figure A-1. Drawing of single molecule of  $K^+(C222).e^-$ .

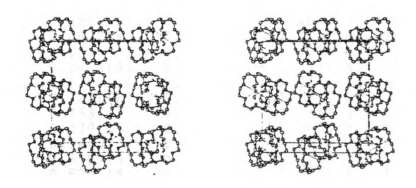


Figure A-2. Stereoview of the unit cell of  $K^+(C222).e^-$ .

Table B-1 Table of Positional Parameters and Their Estimated Standard Deviations for Cesium (18-Crown-6)<sub>2</sub> Ceside

Atom x y z	B(Å <sup>2</sup> )
Cs1         0.34763(4)         0.42001(3)         0.36264(2)           Cs2         0.35442(8)         0.42456(9)         0.09779(3)           O1         0.4636(5)         0.5064(4)         0.4312(2)           O4         0.5077(5)         0.5372(4)         0.3433(3)           O7         0.3824(5)         0.5604(4)         0.2809(2)           O10         0.2260(5)         0.4780(4)         0.2890(2)           O13         0.1829(4)         0.5353(3)         0.3710(2)           O16         0.3044(5)         0.5816(4)         0.4324(2)           O21         0.2389(5)         0.3601(4)         0.4383(2)           O24         0.1887(5)         0.2994(4)         0.3561(3)           O27         0.3060(5)         0.2581(4)         0.2921(2)           O30         0.4609(6)         0.3390(4)         0.2906(3)           O33         0.5152(5)         0.3048(4)         0.3755(3)           O36         0.3970(5)         0.2826(4)         0.4142(5)           C3         0.5552(8)         0.5658(7)         0.3771(4)           C5         0.5151(7)         0.5891(6)         0.3072(4)           C6         0.4660(8)         0.5557(6)         0.2720(4) <td>13.94(4) 7.9(2) 7.2(2) 6.4(2) 6.4(2) 6.6(2) 7.5(2) 7.5(2) 7.5(2) 7.5(2) 9.1(2) 8.4(2) 7.2(2) 11.2(5) 10.5(4) 8.6(4) 7.3(3) 8.6(4) 7.3(3) 8.7(4) 10.6(4) 9.5(4) 9.1(4) 9.5(4) 9.1(4) 11.8(5) 11.9(5) 11.8(5) 11.9(5) 11.8(5) 11.9(5) 11.8(5) 11.9(5)</td>	13.94(4) 7.9(2) 7.2(2) 6.4(2) 6.4(2) 6.6(2) 7.5(2) 7.5(2) 7.5(2) 7.5(2) 9.1(2) 8.4(2) 7.2(2) 11.2(5) 10.5(4) 8.6(4) 7.3(3) 8.6(4) 7.3(3) 8.7(4) 10.6(4) 9.5(4) 9.1(4) 9.5(4) 9.1(4) 11.8(5) 11.9(5) 11.8(5) 11.9(5) 11.8(5) 11.9(5) 11.8(5) 11.9(5)

Starred atoms were refined isotropically. Anisotropically refined atoms are given in the form of the isotropic equivalent thermal parameter defined as:

 $<sup>(4/3) * [</sup>a^2*B(1,1) + b^2*B(2,2) + c^2*B(3,3) + ab(cos gamma)*B(1,2) + ac(cos beta)*B(1,3)$ 

<sup>+</sup> bc(cos alpha)\*B(2,3)

Table B-2

Table of Bond Distances (in Angstroms) for Cesium (18-Crown-6)<sub>2</sub> Ceside

Atom1	Atom2	Distance
Cs1 Cs1 Cs1 Cs1 Cs1 Cs1 Cs1 Cs1 Cs1 Cs1	01 04 07 010 013 016 021 024 027 030 033 036 C2 C18 C5 C6 C8 C9 C112 C12 C14 C15 C17 C22 C38	3.185(8) 3.283(7) 3.486(6) 3.178(7) 3.281(7) 3.503(6) 3.113(7) 3.252(7) 3.516(7) 3.197(8) 3.332(7) 3.444(7) 1.44(2) 1.405(13) 1.391(15) 1.420(13) 1.387(15) 1.420(14) 1.404(13) 1.404(13) 1.404(13) 1.444(12) 1.397(14) 1.437(13) 1.394(15) 1.443(13)
024	C23	1.422(15)

Table B-2 (continued)

Table	of Bond Distances (Continued)	for	
Cesium (18-Crown-6) <sub>2</sub> Ceside			

C25	1.424(13)
	1.382(15)
	1.431(15)
	1.398(14)
	1.41(2)
C32	1.43(2)
C34	1.368(14)
C35	1.436(15)
C37	1.389(14)
C3	1.49(2)
C6	1.46(2)
C9	1.47(2)
C12	1.477(15)
C15	1.51(2)
C18	1.48(2)
C23	1.50(2)
C26	1.49(2)
C29	1.44(2)
C32	1.47(2)
C35	1.47(2)
C38	1.48(2)
	C34 C35 C37 C3 C6 C9 C12 C15 C18 C23 C26 C29 C32

Numbers in parentheses are estimated standard deviations in the least significant digits.

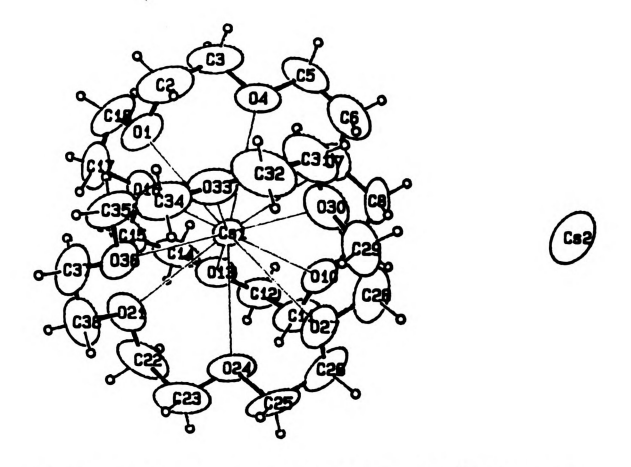


Figure B-1. Drawing of single molecule of  $\mathrm{Cs}^+(18\mathrm{C6})_2.\mathrm{Cs}^-$ .

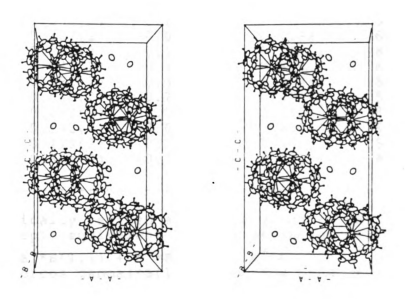


Figure B-2. Stereoview of the unit cell of  $Cs^{+}(18C6)_{2}$ .  $Cs^{-}$ .

TABLE C-1 Table of Positional Parameters and Their Estimated Standard Deviations for Cesium Cryptand [2.2.2] Ceside

Atom	<b>x</b> -	<u>y</u>	<b>z</b> -	B(Å <sup>2</sup> )
Cs1 Cs2 O4 O7 O13 O16 O21 O24 N1 N10 C2 C3 C5 C6 C8 C9 C11 C12 C14 C15 C17 C18 C19 C20 C22 C23 C25 C26	0.2363(1) 0.7442(2) 0.345(1) 0.459(1) 0.082(1) 0.114(1) 0.117(1) 0.345(2) 0.187(1) 0.293(2) 0.444(2) 0.496(2) 0.453(2) 0.453(2) 0.453(2) 0.332(2) 0.332(2) 0.107(2) 0.068(2) 0.068(2) 0.082(2) 0.082(2) 0.082(2) 0.082(2) 0.082(2) 0.172(2) 0.279(2) 0.304(2)	0.0587(2) 0.0689(3) 0.276(1) 0.063(2) -0.136(1) 0.066(2) 0.155(2) -0.081(1) 0.290(2) -0.178(2) 0.379(2) 0.376(2) 0.376(2) 0.376(2) 0.158(2) -0.048(2) -0.146(2) -0.254(2) -0.254(2) -0.254(2) -0.254(2) -0.254(2) -0.254(2) -0.254(2) -0.132(2) -0.132(2) -0.132(2) -0.149(2) -0.149(2) -0.231(2)	0.58667(7) 0.8196(1) 0.6304(7) 0.5946(7) 0.6801(7) 0.6780(6) 0.4818(7) 0.4703(6) 0.6012(8) 0.5732(9) 0.629(1) 0.608(1) 0.615(1) 0.635(1) 0.615(1) 0.625(1) 0.649(1) 0.7288(9) 0.696(1) 0.7288(9) 0.696(1) 0.7288(1) 0.432(1) 0.432(1) 0.432(1) 0.4214(9) 0.461(1) 0.513(1)	3.97(3) 9.60(7) 4.9(4) 5.6(4) 5.1(4) 6.1(5) 5.3(4) 4.7(5) 6.1(6) 4.6(6) 7.4(8) 7.4(8) 7.4(8) 7.5(8) 6.9(8) 7.5(8) 5.9(8) 5.9(8) 5.9(8) 5.9(8) 5.9(8) 5.9(8) 5.9(8) 5.9(8) 5.9(8)
	· •			

Anisotropically refined atoms are given in the form of the isotropic equivalent thermal parameter defined as:

 $<sup>(4/3) * [</sup>a^2*B(1,1) + b^2*B(2,2) + c^2*B(3,3) + ab(cos gamma)*B(1,2) + ac(cos beta)*B(1,3) + bc(cos alpha)*B(2,3)]$ 

TABLE C-2

Table of Bond Distances (in Angstroms) for Cesium Cryptand [2.2.2] Ceside

Atom1	Atom2	Distance
Cs1 Cs1 Cs1 Cs1 Cs1 Cs1 Cs1 Cs1 Cs1 Cs1	04 07 013 016 021 024 N1 N10 C3 C5 C6 C12 C15 C22 C15 C22 C18 C19 C15 C15 C26 C12 C22 C23 C23 C23 C23 C23 C23 C23 C23 C2	2.959(15) 2.972(14) 2.99(2) 2.967(14) 2.888(15) 2.974(14) 3.08(2) 3.06(2) 1.39(3) 1.41(3) 1.39(3) 1.44(3) 1.39(3) 1.46(4) 1.43(3) 1.46(4) 1.43(3) 1.46(3) 1.49(3)
C25	C26	1.52(4)

Numbers in parentheses are estimated standard deviations in the least significant digits.

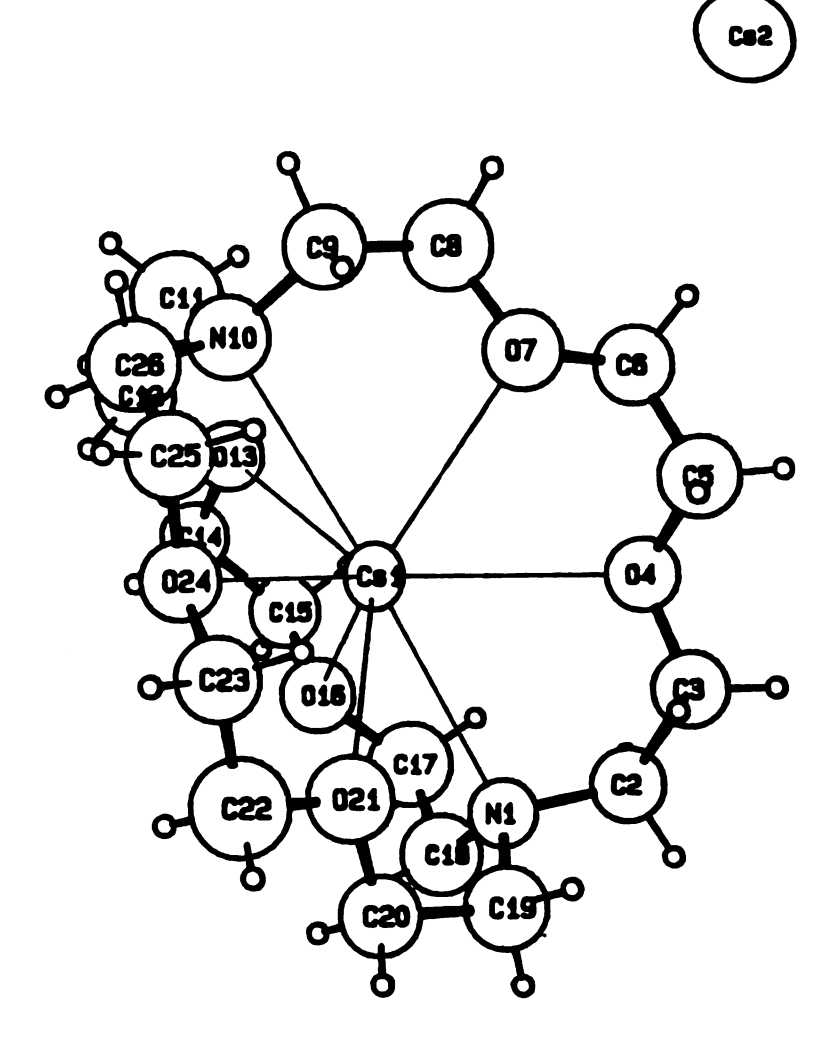


Figure C-1. Drawing of single molecule of Cs<sup>+</sup>(C222).Cs<sup>-</sup>.

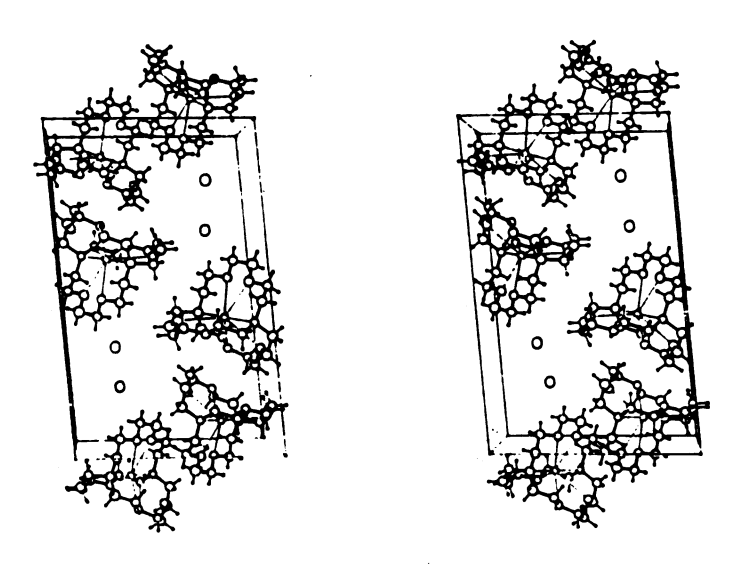


Figure C-2. Stereoview of the unit cell of Cs<sup>+</sup>(C222).Cs<sup>-</sup>.

TABLE D-1 Table of Positional Parameters and Their Estimated Standard Deviations for Rubidium Cryptand[2.2.2] Rubidide

Atom	<b>x</b> -	<u>y</u>	<b>z</b> `	B(Å <sup>2</sup> )
Rb1(+) Rb2(-) O4 O7 O13 O16 O21 O24 N1 N10 C2 C3 C5 C6 C8 C9 C11 C12 C14 C15 C17 C18 C19 C20 C22 C23 C25	-0.1561(1) 0.5357(2) -0.3598(8) -0.3200(8) 0.0653(8) 0.0427(8) -0.1622(8) -0.2030(9) -0.165(1) -0.148(1) -0.287(1) -0.339(1) -0.415(1) -0.430(1) -0.430(1) -0.337(1) -0.219(2) -0.023(2) 0.058(1) 0.145(1) 0.145(1) 0.145(1) 0.145(1) 0.153(1) 0.049(1) -0.073(1) -0.228(1) -0.228(1) -0.162(1)	-0.1890(1) 0.3664(2) -0.0203(8) 0.0660(8) -0.2053(8) -0.2229(8) -0.4271(8) -0.3240(8) -0.3240(8) -0.264(1) -0.116(1) -0.180(2) -0.040(1) 0.111(1) 0.126(1) 0.081(1) 0.023(1) -0.162(1) -0.162(1) -0.162(1) -0.269(1) -0.295(1) -0.295(1) -0.295(1) -0.245(2) -0.399(1) -0.451(1) -0.452(1) -0.314(1)	-0.0467(1) 0.6427(2) -0.1442(9) 0.0994(9) 0.0430(9) -0.2076(9) -0.165(1) 0.093(1) -0.315(1) 0.220(1) -0.341(2) -0.271(1) -0.076(2) 0.054(1) 0.224(1) 0.224(1) 0.224(1) 0.246(1) 0.166(1) -0.327(1) -0.358(2) -0.375(1) -0.358(2) -0.279(2) -0.088(2) 0.031(2) 0.210(1)	4.02(3) 10.01(8) 5.4(3) 5.3(3) 5.2(3) 6.5(3) 6.5(4) 6.5(4) 6.3(4) 7.4(6) 6.8(5) 6.8(5) 7.4(6) 7.4(6) 7.9(6) 7.1(6) 6.2(4) 5.7(4) 6.4(5) 7.4(5) 7.4(5) 7.4(5) 7.3(5)
C26	-0.203(2)	-0.178(1)	0.277(1)	8.6(6)

Anisotropically refined atoms are given in the form of the isotropic equivalent thermal parameter defined as:

 $<sup>(4/3) * [</sup>a^2*B(1,1) + b^2*B(2,2) + c^2*B(3,3) + ab(cos gamma)*B(1,2) + ac(cos beta)*B(1,3) + bc(cos alpha)*B(2,3)]$ 

TABLE D-2 Table of Bond Distances (in Angstroms) for Rubidium Cryptand[2.2.2] Rubidide

Atom1	Atom2	Distance
Rb1	04	2.888(9)
Rb1	07	2.866(7)
Rb1	013	2.853(11)
Rb1	016	2.929(11)
Rb1	021	2.922(10)
Rb1	024	2.869(13)
Rb1	N1	3.002(14)
Rb1	N10	2.976(13)
04	C3	1.43(2)
04	C5	1.420(14)
07	C6	1.39(2)
07	C8	1.41(2)
013	C12	1.41(2)
013	C14	1.40(2)
016	C15	1.40(2)
016	C17	1.40(2)
021	C20	1.41(2)
021	C22	1.41(2)
024	C23	1.42(2)
024	C25	1.44(2)
N1	C2	1.47(2)
N1	C18	1.49(3)
N1	C19	1.49(3) 1.47(2)
N10	C9	1.47(2)
N10	C11	1.45(2)
N10	C26	1.50(3)
C2	C3	1.51(2)
C5	C6	1.48(2)
C8	C9	1.47(2)
C11	C12	1.54(3)
C14	C15	1.46(2)
C17	C18	1.51(2)
C19	C18 C20	1.52(3)
C22	C23	1.49(3)
C25	C26	1.49(2)
CZJ	C20	エ・サフしム丿

Numbers in parentheses are estimated standard deviations in the least significant digits.



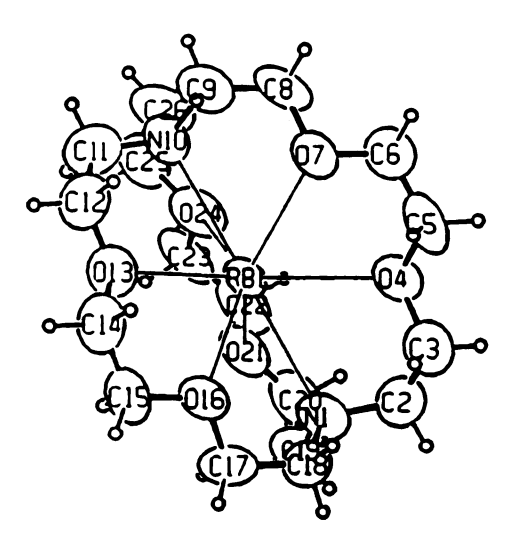


Figure D-1. Drawing of single molecule of Rb<sup>+</sup>(C222).Rb<sup>-</sup>.

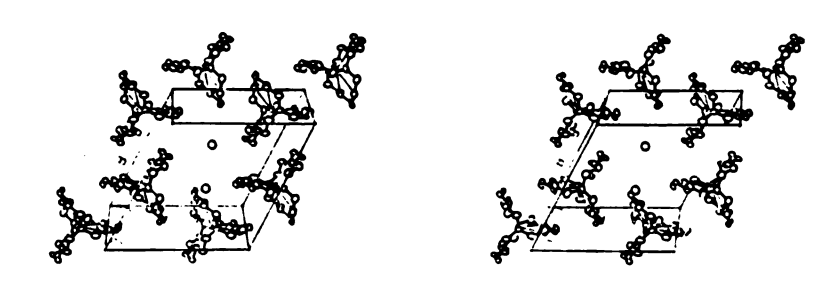


Figure D-2. Stereoview of the unit cell of Rb+(C222).Rb-.

TABLE E-1 Table of Positional Parameters and Their Estimated Standard Deviations for

K<sup>+</sup>(Cryptand[2.2.2]).Na<sup>-</sup>

K1       0.000       0.000       0.000       2.447(9)         Na1       0.000       0.000       0.4151(1)       6.41(4)         04       -0.0007(1)       0.09556(6)       0.0989(1)       4.00(3)         07       -0.1552(1)       0.04284(6)       0.0677(1)       3.85(3)         013       0.06218(9)       0.04014(6)       -0.1801(1)       2.97(3)         N1       0.1544(1)       0.06749(7)       -0.0041(2)       3.33(4)         C2       0.1485(2)       0.10556(9)       0.0771(2)       4.44(5)         C3       0.0643(2)       0.13368(9)       0.0834(2)       4.33(5)         C5       -0.0800(2)       0.1207(1)       0.11457(2)       4.68(6)         C6       -0.1438(2)       0.0792(1)       0.1457(2)       4.68(6)         C8       -0.2226(2)       0.0064(1)       0.0884(2)       4.59(6)         C9       -0.2300(1)       -0.03334(9)       0.0088(2)       4.31(5)         C11       0.1605(1)       0.09597(9)       -0.0963(2)       3.95(5)         C12       0.1457(1)       0.06197(9)       -0.1840(2)       3.84(5)         C14       0.0458(1)       0.0087(9)       -0.2633(2)       3.49(5)
H14b $0.053(1)$ $0.0303(8)$ $-0.327(2)$ $0.9(5)*$

Starred atoms were refined isotropically.
Anisotropically refined atoms are given in the form of the isotropic equivalent thermal parameter defined as:

 $<sup>(4/3) * [</sup>a^2*B(1,1) + b^2*B(2,2) + c^2*B(3,3) + ab(cos gamma)*B(1,2) + ac(cos beta)*B(1,3)$ 

<sup>+</sup> bc(cos alpha)\*B(2,3)

TABLE E-2 Table of Bond Distances (in Angstroms) for K<sup>+</sup>(Cryptand[2.2.2]).Na<sup>-</sup>

Atom1	Atom2	Distance
K1 K1	04 07	2.773(2) 2.835(2)
K1	013	2.860(2)
K1	04'	2.773(2)
K1 K1	07'	2.834(2) 2.860(2)
K1	013' N1	2.860(2)
K1	N1'	2.972(2)
04	C3	1.422(3)
04	C5	1.426(3)
07	C6	1.427(3)
07	C8 C12	1.434(3)
013 013	C12	1.429(3) 1.420(3)
N1	C2	1.480(3)
N1	C11	1.466(3)
N1	C9′	1.482(2)
C2 C5	C3 C6	1.509(4)
C5		1.506(4)
C8 C11	C9 C12	1.493(4) 1.504(4)
C14	C14'	1.511(2)
C2	H2a	1.01(2)
C2	н2ь	0.96(2)
C3	нЗа	1.01(3)
C3	H3b	1.04(2)
C5 C5	Н5 <b>а</b> Н5b	1.05(2) 0.95(2)
C6	нэв <b>Нба</b>	0.99(2)
C6	н6 <b>Б</b>	0.95(3)
C8	H8a	1.00(2)
C8	н8ь	0.98(2)
C9	н9а	0.99(2)
C9	H9b	1.03(2)
C11 C11	H11a H11b	0.98(2) 0.95(2)
C12	H12a	0.96(2)
C12	H12b	0.99(2)
C14	H14a	1.00(2)
C14	H14b	1.04(2)

Numbers in parentheses are estimated standard deviations in the least significant digits.

' indicates an atom at -X, -Y, Z

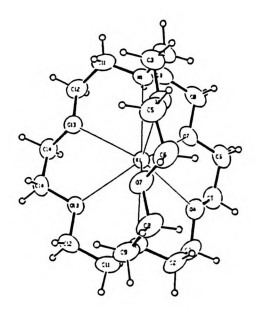


Figure E-1. Drawing of single molecule of K+(C222).Na-.

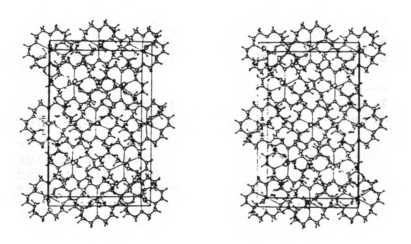


Figure E-2. Stereoview of the unit cell of  $K^+(C222).Na^-$ .

Table F-1 Table of Positional Parameters and Their Estimated Standard Deviations for Cesium (15-Crown-5)<sub>2</sub> Potasside

Atom	<b>x</b> -	<u>y</u>	<b>z</b> -	B(Å <sup>2</sup> )
Cs1 K1 O1 O7 C2 C5 C6 a C8b H2b H3a H3b H5b H6a H8ba H8ba	0.500 0.500 0.4754(7) 0.5141(5) 0.7271(5) 0.4117(8) 0.4872(9) 0.614(1) 0.7228(8) 0.828(1) 0.819(1) 0.369(6) 0.369(6) 0.461(6) 0.543(4) 0.600(6) 0.605(5) 0.778(6) 0.734(6) 0.902 0.816 0.802 0.888	0.000 0.500 0.000 -0.1790(4) -0.1056(4) -0.0877(7) -0.1710(7) -0.2347(6) -0.1789(8) -0.031(1) 0.055(1) -0.073(5) -0.075(5) -0.218(6) -0.218(6) -0.288(5) -0.239(4) -0.209(5) -0.153(6) -0.061 -0.008 0.033 0.091	0.500 0.000 0.2033(8) 0.3301(5) 0.4388(6) 0.1790(8) 0.204(1) 0.3558(9) 0.347(1) 0.470(2) 0.384(2) 0.110(7) 0.237(7) 0.167(4) 0.314(6) 0.420(5) 0.345(6) 0.284(7) 0.465 0.554 0.301 0.384	5.43(2) 5.87(2) 5.87(1) 6.4(2) 7.5(3) 7.8(3) 8.8(4) 6.4(4) 3(2)* 4(2)* 4(2)* 4(2)* 4(2)* 8.7* 8.7* 8.7*
11000	0.000	0.031	0.304	<b>0.</b> / "

Anisotropically refined atoms are given in the form of the isotropic equivalent thermal parameter defined as:

Starred atoms were refined isotropically.

 $<sup>(4/3) * [</sup>a^2*B(1,1) + b^2*B(2,2) + c^2*B(3,3) + ab(cos gamma)*B(1,2) + ac(cos beta)*B(1,3) + bc(cos alpha)*B(2,3)]$ 

Table F-2

Table of Bond Distances (in Angstroms) for Cesium (15-Crown-5)<sub>2</sub> Potasside

Atom1	Atom2	Distance
Cs1	01	3.171(8)
Cs1	04	3.056(5)
Cs1	07	3.078(5)
01	C2	1.436(10)
04	C3	1.383(12)
04	C5	1.418(12)
07	C6	1.400(12)
07 <u>.</u>	C8a	1.593(14)
07 <sup>i</sup>	C8b	1.403
C2	C3	1.463(13)
C5	C6	1.476(14)
C8a	C8p	1.50(2)
C2	H2a	0.79(7)
C2	H2b	0.82(7)
C3	нЗа	0.76(8)
C3	H3b	0.79(5)
C5	H5a	0.87(7)
C5	н5ь	0.69(6)
C6	Нба	0.76(7)
C6	н6Ь	0.77(8)
C8a	H8aa	0.95
C8a	H8ab	0.95
C8b	H8ba	0.95
C8b	H8bb	0.95
CUD	11000	0.33

Numbers in parentheses are estimated standard deviations in the least significant digits.

indicates an atom at x, -y, z

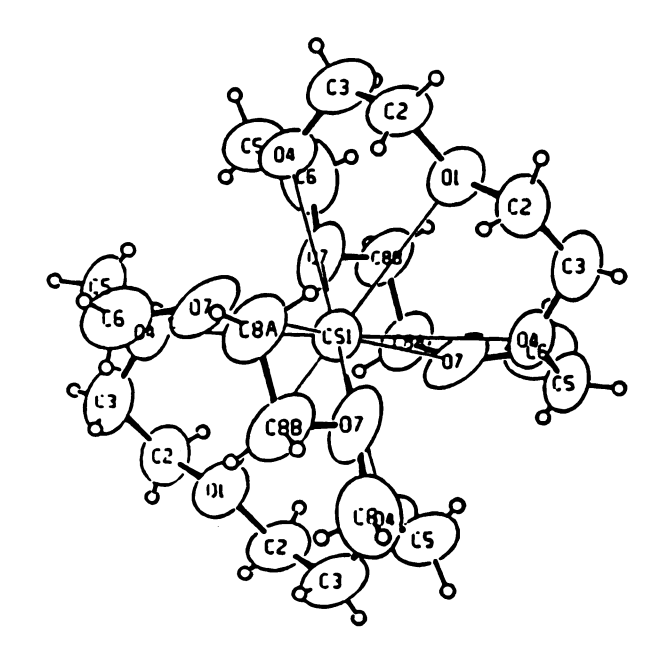


Figure F-1. Drawing of single molecule of  $Cs^+(15C5)_2.K^-$ .

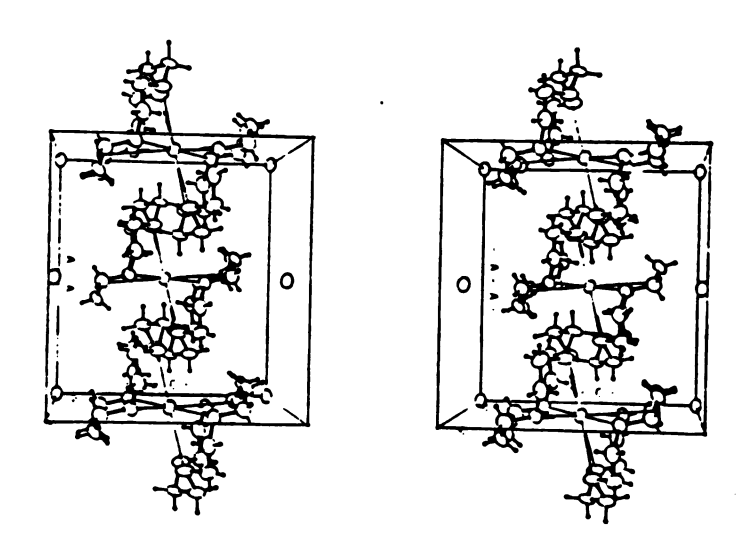


Figure F-2. Stereoview of the unit cell of  $Cs^+(15C5)_2.K^-$ .

## Appendix 2.

Explanation of the entries in the tables of crystal data.

- Temperature the temperature of the single crystal on the x-ray diffractometer.
- Peak width at half-height the width of the peak of a standard reflection at the half-height of the peak.
- 3. Scan type the mode of scan during the data collection.
  The angle between the x-ray beam and the detector is
  2theta.
- 4. Scan rate the rate with which the angle (2theta or omega) is scanned during the data collection.
- 5. Unique reflections the reflections which are not related by the symmetry of the reciprocal lattice.
- 6. Corrections the corrections made to the intensities of reflections.
- 7. Solution the method for solving the structure.
- 8. Hydrogen atoms the way the hydrogen atoms were treated during the refinement.
- 9. R the residual index.  $R = \sum |F_O F_C| / \sum F_O$ , where  $F_O$  is the structure factor related to the intensity observed,  $F_C$  is the structure factor calculated. The sum is over all the reflections used in the refinement.
- 10.  $R_{\omega}$  the weighted residual index.

$$R_W = SQRT[\Sigma w(F_O - F_C)^2 / \Sigma w F_O^2]$$
 and

$$w = 4F_0^2 / [sigma(F_0^2)]^2$$

- 11. High peak in final difference map the highest peak in the final difference electron density map.
- 12. Standard deviation of observation of unit weight it is calculated by the formula

$${\tt SQRT[(\Sigma w(F_O^{-}F_C)^2)/(N_1^{-}N_2^{})]}$$

where  $N_1$  is the number of the observed reflections used in the refinement and  $N_2$  is the number of parameters in the refinement.

13. Convergence, largest shift - the largest of shifts of parameters during the final refinement cycle. LIST OF REFERENCES

## LIST OF REFERENCES

- 1. J. L. Dye, J. M. Ceraso, M. T. Lok, B. L. Barnett and F. J. Tehan, <u>J. Am. Chem. Soc.</u>, <u>96</u>, 608 (1974).
- 2. F. J. Tehan, B. L. Barnett and J. L. Dye, <u>J. Am. Chem.</u> Soc., <u>96</u>, 7203 (1974).
- 3. J. L. Dye, Prog. Inorg. Chem., 32, 327 (1984).
- 4. J. L. Dye, Scientific American, 257, 66 (1987).
- 5. J. L. Dye, and M. G. DeBacker, <u>Ann. Rev. Phys. Chem.</u>, <u>38</u>, 271, (1987)
- 6. S. B. Dawes, D. L. Ward, R. H. Huang and J. L. Dye, <u>J. Am. Chem. Soc.</u>, <u>108</u>, 3534 (1986).
- 7. S. B. Dawes, Ph.D Dissertation, Michigan State University (1986).
- 8. O. Fussa, Ph.D Dissertation, Michigan State University (1986)
- 9. J. Papaioannou, S. Jaenicke and J. L. Dye, <u>J. Solid State</u> Chem., <u>67</u>, 122 (1987).
- S. Jaenicke and J. L. Dye, <u>J. Solid State Chem.</u>, <u>54</u>, 320 (1984).
- 11. J. L. Dye, R. H. Huang and D. L. Ward, submitted for publication.
- 12. R. H. Huang, D. L. Ward, M. E. Kuchenmeister and J. L. Dye, <u>J. Am. Chem. Soc.</u>, in press.
- 13. R. H. Huang, M. K. Faber, K. J. Moeggenborg and J. L. Dye, submitted for publication.
- 14. A. Ellaboudy, Ph.D Dissertation, Michigan State University (1984).
- 15. M. K. Faber, Ph.D dissertation, Michigan State University (1985).
- 16. J. S. Landers, Ph.D Dissertation, Michigan State University (1981).

- 17. A. Ellaboudy, J. L. Dye and P. B. Smith, <u>J. Am. Chem. Soc.</u>, <u>105</u>, 6490 (1983).
- 18. D. Issa, A. Ellaboudy, R. Janakiraman and J. L. Dye,  $\underline{J}$ . Phys. Chem., 88, 3847 (1984).
- 19. S. B. Dawes, D. L. Ward, O. Fussa and J. L. Dye, Abstracts, Am. Crys. Asso. Proc., Series 2, Vol. 13, 25 (1985)
- 20. P. Moras, B. Metz, R. Weiss, <u>Acta Cryst.</u>, Sect. <u>B</u>, <u>B29</u>, 388 (1973).
- 21. K. P. Huber and G. Herzberg, "Molecular Spectra and Molecular Structure" IV. "Constants of Diatomic Molecules", Van Nostrand Reinhold Company, New York (1979).
- 22. G. Igel-Mann, U. Wedig, P. Fuentealba and H. Stoll, <u>J. Chem. Phys.</u>, <u>84</u>, 5007 (1986).
- 23. P. D. Moras, B. Metz and R. Weiss, <u>Acta Cryst.</u>, <u>B29</u>, 383 (1973).
- 24. M. L. Tinkham and J. L. Dye, <u>J. Am. Chem. Soc.</u>, <u>107</u>, 6129 (1985).
- 25. M. L. Tinkham, A. Ellaboudy, J. L. Dye and P. B. Smith, J. Phys. Chem., 90, 14 (1986).
- 26. D. L. Ward, R. H. Huang and J. L. Dye, submitted for publication.
- 27. O. Fussa, S. Kauzlarich, J. L. Dye and B. K. Teo,  $\underline{J.\ Am}$ . Chem. Soc.,  $\underline{107}$ , 3727(1985).
- 28. D. W. Turner, C. Baker, A. D. Baker and C. R. Brundle, "Molecular Photoelectron Spectroscopy", Witey-Interscience, London (1970).
- 29. K. Kimura, S. Katsumata, Y. Achiba, T. Yamazaki and S. Iwata, " <u>Handbook of HeI Photoelectron Spectra of Fundamental Organic Molecules</u>", Japan Scientific Societies Press, Tokyo (1981).
- 30. P. Delahay in "Electron Spectroscopy. Theory, Techniques and Applications", Vol. 5, C. R. Brundle and A. D. Baker edited, Academic Press, New York (1984).
- 31. M. Cardona and L. Ley, "Photoemission in Solids I", Spinger-Verlag, New York (1978).
- 32. B. Feuerbacher, B. Fitton and R. F. Wills, "Photoemission and the Electronic Properties of Surfaces", John Wiley & Sons, New York (1978).

- 33. H. Widdawi and F. F.-L. Ho, "Applied Electron Spectroscopy for Chemical Analysis", John Wiley and Sons, New York (1982).
- 34. P. K. Ghosh, " <u>Introduction to Photoelectron</u> <u>Spectroscopy</u> ", John Wiley and Sons, New York (1983).
- 35. D. Briggs, " <u>Handbook of X-Ray and Ultraviolet</u> <u>Photoelectron Spectroscopy</u> ", Heyden and Son Ltd., London (1977).
- 36. H. Hertz, Ann. Physik, 31, 983 (1887).
- 37. A. Einstein, Ann. Physik, 17, 132 (1905).
- 38. C. R. Brundle and A. D. Baker, " <u>Electron Spectroscopy:</u> <u>Theory, Techniques and Applications</u> ", Vol. 1, Acadamic Press, London (1977).
- 39. H. A. Wilson, Phil. Trans. (A), 197, 429 (1901).
- 40. A. L. Reimann, "Thermionic Emission", John Wiley & Sons, New York (1934).
- 41. N. Gremmo and J. E. B. Randles, <u>J. Chem. Soc.</u>, <u>Faraday</u> <u>Trans. 1</u>, <u>70</u>, 1488 (1974).
- 42. R. V. Coleman, "Methods of Experimental Physics", V.11, "Solid State Physics", Academic Press, New York (1974).

